Experimental Investigation on Effect of Print Orientation on Mechanical and Tribological Behavior of 3D Printed Carbon Fiber Reinforced Polyamide-6

Rediet Getahun

A Thesis Submitted to the Department of Mechanical Engineering,

School of Mechanical, Chemical, and Material Engineering

Presented in Partial Fulfillment of the Requirement for the Degree of Master's in Manufacturing Engineering

Office of Graduate Studies

Adama Science and Technology University

June, 2024
Adama, Ethiopia

Experimental Investigation on Effect of Print Orientation on Mechanical and Tribological Behavior of 3D Printed Carbon Fiber Reinforced Polyamide-6

Rediet Getahun

Advisor: Dr. G.M. Sayeed Ahmed (PhD),

Associate Professor

A Thesis Submitted to the Department of Mechanical Engineering,

School of Mechanical, Chemical, and Material Engineering

Presented in Partial Fulfillment of the Requirement for the Degree of Master's in Manufacturing Engineering

Office of Graduate Studies

Adama Science and Technology University

June, 2024

Adama, Ethiopia

DECLARATION

I hereby declare that this Master Thesis entitled "Experimental Investigation on Effect of Print Orientation on Mechanical and Tribological Behavior of 3D Printed Carbon Fiber Reinforced Polyamide-6'' is my original work. That is, it has not been submitted for the award of any academic degree, diploma, or certificate in any other university. All sources of materials that are used for this thesis have been duly acknowledged through citation.

Rediet Getahun	______________	______________
Name of student	Signature	Date

RECOMMENDATION

I, the advisor of this thesis, hereby certify that I have read the revised version of the thesis entitled "Experimental Investigation on Effect of Print Orientation on Mechanical and Tribological Behavior of 3D Printed Carbon Fiber Reinforced Polyamide-6" prepared under my guidance by Rediet Getahun submitted in partial fulfillment of the requirements for the degree of Mater's of Science in Manufacturing Engineering. Therefore, I recommend the submission of a revised version of the thesis to the department following the applicable procedures.

Dr. G.M. Sayeed Ahmed (Ph.D.)	__________________	__________________
Major Advisor/Supervisor	Signature	Date

APPROVAL SHEET

I, the advisor of the thesis entitled "Experimental Investigation on Effect of Print Orientation on Mechanical and Tribological Behavior of 3D Printed Carbon Fiber Reinforced Polyamide-6" and developed by Rediet Getahun, hereby certify that the recommendation and suggestions made by the board of examiners are appropriately incorporated into the final version of the thesis.

Dr. G.M. Sayeed Ahmed (Ph.D.)	____________________	_________________
Major Advisor/Supervisor	Signature	Date

APPROVAL OF BOARD OF REVIEWERS

We, the undersigned, members of the Board of Examiners of the thesis by Rediet Getahun have read and evaluated the thesis entitled "Experimental Investigation on Effect of Print Orientation on Mechanical and Tribological Behavior of 3D Printed Carbon Fiber Reinforced Polyamide-6'' and examined the candidate during open defense. This is, therefore, to certify that the thesis is accepted for partial fulfillment of the requirement of the degree of Master of Science in Manufacturing Engineering.

____________________	____________	____________
Chairperson	Signature	Date
____________________	____________	____________
Internal Examiner	Signature	Date
____________________	____________	____________
External Examiner	Signature	Date

Final approval and acceptance of the thesis is contingent upon submission of its final copy to the Office of Postgraduate Studies (OPGS) through the Department Graduate Council (DGC) and School Graduate Committee (SGC).

____________________	____________	____________
Department Head	Signature	Date
____________________	____________	____________
School Dean	Signature	Date
____________________	____________	____________
Office of Postgraduate Studies, Dean	Signature	Date

ACKNOWLEDGMENT

First and foremost, I would like to express my deepest gratitude to God for granting me the strength, wisdom, and perseverance to complete this thesis. Without His guidance and blessings, this work would not have been possible. I would also like to extend my heartfelt appreciation to my advisor Dr. G.M. Sayeed Ahmed for their unwavering support, guidance, and encouragement throughout this journey. Your insightful feedback and invaluable advice have been instrumental in shaping this research. Thank you for believing in my potential and for being a constant source of inspiration. My sincere thanks go to Adama Science and Technology University for providing me with the opportunity and resources to pursue my studies. The knowledge and experiences gained here have been truly enriching and will stay with me for a lifetime. I am immensely grateful to my friends for their companionship, encouragement, and the countless memorable moments we have shared. Your support has been a cornerstone during the challenging times of this journey. Lastly, I would like to acknowledge my family for their unconditional love and support. Your faith in me has been a driving force behind my achievements, and I am forever grateful for your presence in my life.

Thank you all for your contributions and support in making this thesis a reality.

TABLE OF CONTENTS

LIST OF TABLES

LIST OF FIGURES

ABBREVIATIONS AND ACRONYMS

3D	3-Dimensional
ANOVA	Analysis of Variance
AM	Additive Manufacturing
ASTM	American Society for Testing and Materials
CAD	Computer-Aided Design
CF	Carbon Fibers
CFRPs	Carbon Fiber Reinforced Polymers
CFRPA	Carbon Fiber Reinforced Polyamide
COF	Coefficient of Friction
DOE	Design of Experiment
FDM	Fused Deposition Modeling
FFF	Fused Filament Fabrication
GRA	Grey Relational Analysis
GRG	Grey Relational Grade
HV	Vickers Hardness
L	Load
PA	Polyamide
p-value	Probability value
SEM	Scanning Electron Microscopy
SS	Sliding Speed
STL	Stereo Lithography
TD	Track Diameter
UTM	Universal Testing Machine

ABSTRACT

Additive manufacturing (AM) is revolutionizing the production of complex and customized components across various industries. Among the materials used in AM, carbon fiber-reinforced polyamide (CFRPA) stands out due to its exceptional mechanical properties and lightweight nature. However, the mechanical and tribological properties of 3D-printed parts can be significantly influenced by the print orientation. The purpose of this research was to investigate the effect of print orientation (horizontal, vertical, and 45 degrees) on the mechanical and tribological properties of CFRPA6 and to optimize wear parameters to enhance the performance of the material. The samples were fabricated using the fused filament fabrication process (FFF). Experimental testing was conducted to evaluate the mechanical properties, including tensile strength, hardness, physical properties (density and porosity), and tribological properties such as wear and friction. The study findings indicate that sliding speed has the most significant impact on wear and friction characterization, followed by load and track diameter. Scanning electron microscopy was used to study microstructural changes and surface morphology. *The optimum results of wear characterization for horizontal, vertical, and 45-degree orientation were wear rates (2.23, 3.23, and 2.45). * 10^{-3} mm^3/m and hardness results were (81.6, 57.86, and 72.73) HV respectively. The vertical orientation demonstrates the highest tensile strength (0.046 MPa), the 45-degree orientation (0.02 MPa), and the horizontal orientation (0.019 MPa). The porosity test showed that horizontal orientation had a relatively lower porosity percentage. The LS-DYNA simulation result showed that horizontal orientation had less stress and deformation. It was concluded that horizontally printed CFRPA6 has high hardness and low porosity, resulting in a low wear rate and COF, making it ideal for wear-resistant applications. Vertical prints, with better tensile strength, are suitable for applications requiring higher tensile strength.*

Keywords: *Print orientation, CFRPA, FFF, mechanical property, wear, LS-DYNA software*

CHAPTER ONE

INTRODUCTION

1.1 Background of the Study

Additive manufacturing (AM) is the method of producing items directly from a computer-aided design (CAD) by layering materials on top of each other (Dangnan et al., 2020). AM technology is closely associated with Industry 4.0 and revolutionizes manufacturing and production methods. AM can streamline various fabrication processes by minimizing raw material usage, while simultaneously enhancing the properties of the end product in terms of functionality and weight (Espadinha-Cruz et al., 2023). The primary goal of AM is to minimize process time and steps, which can be achieved through rapid prototyping technologies. AM is a vital manufacturing technology for fabricating metallic and polymer parts (Naik et al., 2022).

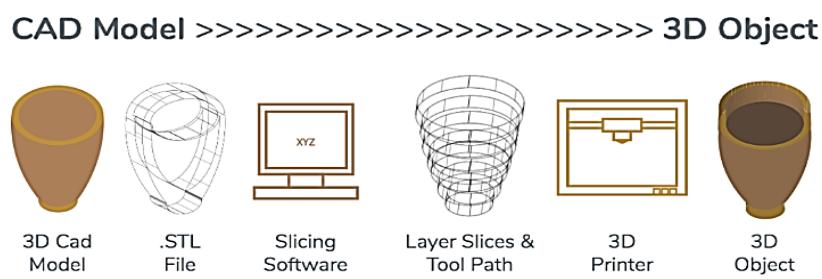

Figure1-1: Additive manufacturing process

In the fabrication process of a 3D object, successive layers are laid down starting from various forms of liquid, powder, or sheet materials by using an AM machine (Dul et al., 2021). The 3D model undergoes layer division (slicing), the establishment of construction orientation, the definition of support structures required for layer deposition in near-horizontal orientations, and the determination of the manufacturing path or sequence. These processes are executed using specialized software tailored to the technology and occasionally specified by the printer brand, representing a second possible source of deviation or alteration from the original data. Consequently, variations in orientation, support structure, or manufacturing sequence can lead to differences in the final piece produced. The AM of reinforced polymer-based composites typically employs extrusion-based techniques, with Fused Filament Fabrication (FFF) being the commonly adopted method for processing polymers (Dhakal et al., 2024). The FFF process is carried out with an automated apparatus laying down molten thermoplastic filaments and relying on fusing them to form a part (Abderrafai et al., 2022).

Polymers provide unlimited flexibility to produce polymer composites at relatively lower material and processing costs than metals, alloys, and ceramics (Al Rashid et al., 2022). Among available potential triboengineering polymers, polyamides (PA) can be highlighted (Pereira & d'Almeida, 2023). PA is a semi-crystalline thermoplastic considered as a good candidate thermoplastic composite matrix, mainly due to its low cost and easy handling. Polymer materials provide a high strength/weight ratio in comparison to classic material and self-lubricant conditions. However, applications of classic polymer materials are limited due to their low mechanical, thermal, and tribological properties making the use of polymers alone has resulted in limited applications. Therefore, reinforcements are used to improve their properties (tribological, thermal, and mechanical properties) (Naik et al., 2022).

Carbon fibers (CF) are a crucial reinforcement for structural uses due to their exceptionally high specific mechanical properties (properties relative to material density) and their widespread availability in forms such as continuous fibers, woven fabrics, or short fibers (Abderrafai et al., 2022). Carbon fiber-reinforced polymers (CFRPs) are composite materials with high strength and lightweight that are made of CFs and a polymer matrix. The carbon fiber additives can improve the wear resistance of polymeric matrix by increasing the loading capacity.

The use of CFRPs has proven advantageous in applications with demanding contact wear. To meet tribological requirements, polymers must exhibit superior wear resistance. Polymers tend to have a short lifespan and limited load-bearing capacity under high load and speed conditions. Composites can offer up to 40% weight savings for secondary structures compared to light metal alloys, and up to 20% weight savings for primary structures like wings and fuselages. Additionally, frictional interactions between micro-components are increasingly important for the development of new products in modern industries (Krishna Vamsi et al., 2022). To investigate the multiple attributes associated with the wear resistance of composites, a range of decision-making techniques, such as analytic hierarchy process (AHP), data envelopment analysis (DEA), grey relational analysis (GRA), and technique for order of preference by similarity to ideal solution (TOPSIS), have been suggested in the literature. Among them, grey relational analysis (GRA), proposed by Deng in 1989, is one of the foremost techniques applied when the nature of information is incomplete and uncertain (Sylajakumari et al., 2018).

1.2 Application Area of 3D printed CFRP

Carbon fiber reinforced polyamide (CFRP) composites have a wide range of applications due to their high strength, low weight, and excellent thermal and electrical properties. Because of their high strength-to-weight ratio and stiffness, these materials are widely employed in aircraft, automotive, civil engineering, sports equipment, and a growing range of consumer and technical applications. Aircraft fuselages, wings, and tail sections are examples of structural components in the aerospace sector. Their excellent strength-to-weight ratio makes them ideal for decreasing aircraft weight while increasing fuel economy. Additionally, it is used to make lightweight auto parts such as body panels, chassis components, and suspension systems. This improves vehicle fuel efficiency and performance (Kausar, 2019).

1.3 Statement of the Problem

The growing demand for lightweight, durable, and wear-resistant components in industries such as aerospace, automotive, and robotics has driven the adoption of CFRPs**.** Additive manufacturing, particularly fused deposition modeling (FDM), has emerged as a promising technique for fabricating CFRPs parts with complex geometries. However, the mechanical and tribological performance of 3D printed material is greatly influenced by the printing parameters during the manufacturing process. The anisotropic nature of printed parts results in significant variations in their tensile strength, hardness, wear resistance, and coefficient of friction depending on the print orientation. Without a clear understanding of how print orientation affects these properties, components may experience reduced lifespan, unexpected failures, and inconsistent performance, leading to increased maintenance costs and potential safety hazards. Identifying these effects is crucial for optimizing design and manufacturing processes to ensure that the designed parts meet the stringent requirements of their intended applications, such as high-stress environments in automotive gears or aerospace brackets where both lightweight and high durability are paramount.

1.4 Research Questions

The following research questions are designed to explore the effects of different print orientations on the property of CFRPA:

1. How does print orientation affect mechanical property and tribological properties in dry sliding conditions?
2. What is the optimal sliding speed, load, and track diameter to minimize wear for different print orientations?
3. What is the comparative effect of print orientation on density and porosity?
4. Which print orientation minimizes stress concentrations and maximizes deformation resistance?

1.5 Objective of the Study

1.5.1 General objective

The main objective of this thesis was to experimentally investigate the effect of print orientation on the mechanical and tribological behavior of 3D-printed carbon fiber-reinforced polyamide.

1.5.2 Specific objectives

The specific objectives are as follows:

1. To investigate the influence of print orientation on mechanical, physical, and tribological properties.
2. To investigate optimum wear parameters (load, sliding speed, and track diameter) using Taguchi-based grey analysis.
3. To study microstructural changes and surface morphology using SEM.
4. To analyze the effect of print orientation on stress and deformation using LS-DYNA simulation software.

1.6 Significance of the Study

Considering how printing orientation influences mechanical and tribological qualities, this enables the adjustment of 3D orientation components to improve performance in specific applications. For instance, knowing which orientation yields the highest tensile strength or the best wear resistance can help in designing parts that are more durable and reliable. Optimizing wear test parameters ensures that the testing process is efficient and provides reliable data, including identifying the best conditions (e.g., load, speed, track diameter) under which the material performs optimally. This understanding allows for more effective use of CFRPA6, potentially reducing material wastage and improving cost-efficiency. The findings can be used by researchers and engineers to further refine and advance the technology and its applications, leading to better control over the quality of the final product.

1.7 Scope of the Study

This research aims to investigate the effect of printing orientation (horizontal, vertical, and 45-degree) on the mechanical properties (tensile strength and material hardness) and tribological properties (wear and COF) of CFRPA6. The samples were manufactured using the fused filament fabrication process. Tensile strength was tested using a UTM machine, hardness was tested using Vickers hardness, and wear was tested using a pin-on-disk apparatus. The optimization of wear parameters was conducted for horizontal, vertical, and 45-degree orientations. An experimental design with a Taguchi L9 (3^3) orthogonal array was developed with three controlling factors: applied load, sliding speed, and track diameter. Subsequently, nine experimental runs for each print orientation were conducted to gather data on the wear rate, specific wear rate and COF. Thereafter, S/N ratios and GRA were used to analyze the responses and obtain the optimal parameters. The most significant factors affecting the wear behavior of CFRPA6 were identified using ANOVA. The effect of printing orientation on wear rate, specific wear rate and COF compared. The effect of wear on morphology was characterized using scanning electron microscopy, and stress and deformation were analyzed using LS DYNA software.

1.8 Limitations of the Study

The study primarily focused on the effect of print orientation on the material properties. Other important print parameters such as print speed, nozzle temperature, Cooling Rate and Post-Processing were not analyzed. The tests were conducted under controlled laboratory conditions, which may not accurately represent the operational environments where the materials will be used. Factors such as temperature, humidity, and exposure to chemicals were not considered and could affect the material properties.

1.9 Research Outline

This research paper consists of five chapters, with the key points of each chapter discussed below. The first chapter is an introduction of the study. It covers the background of the research, the problem statement, the objectives, the scope, the limitations of the work, and the organization of the report. Chapter Two summarizes the literature on the properties of CFRP and fabrication process. Chapter Three outlines the materials, methods, and methodology employed to achieve the objectives. Chapter Four presents the results and their discussions, and Chapter Five concludes with recommendations for further research and includes the references and appendices.

CHAPTER TWO

LITERATURE REVIEW

2.1 Introduction

This chapter is a review of the published literature related to the effect of print parameters on 3D print material. The available mechanical and tribological tests and their effects on wear rate, specific wear rate, and coefficient of friction have been discussed. The subsection reviews the previous research done on the effect of print on mechanical and tribological CFRP material.

2.2 Mechanical property of CFRP

The mechanical performance of 3D-orientation composites, like conventional composites, depends on various factors such as the properties of their constituents, the structure of the reinforcement, the bonding between constituents, the amount of reinforcement, and the manufacturing process (Sanei & Popescu, 2020). The mechanical characteristics of polymer composites are affected by factors like the length and volume fraction of fibers, their orientation, and the processing conditions. Ensuring compatibility between fibers and the matrix material is also a significant concern (Lizenboim et al., 2024).

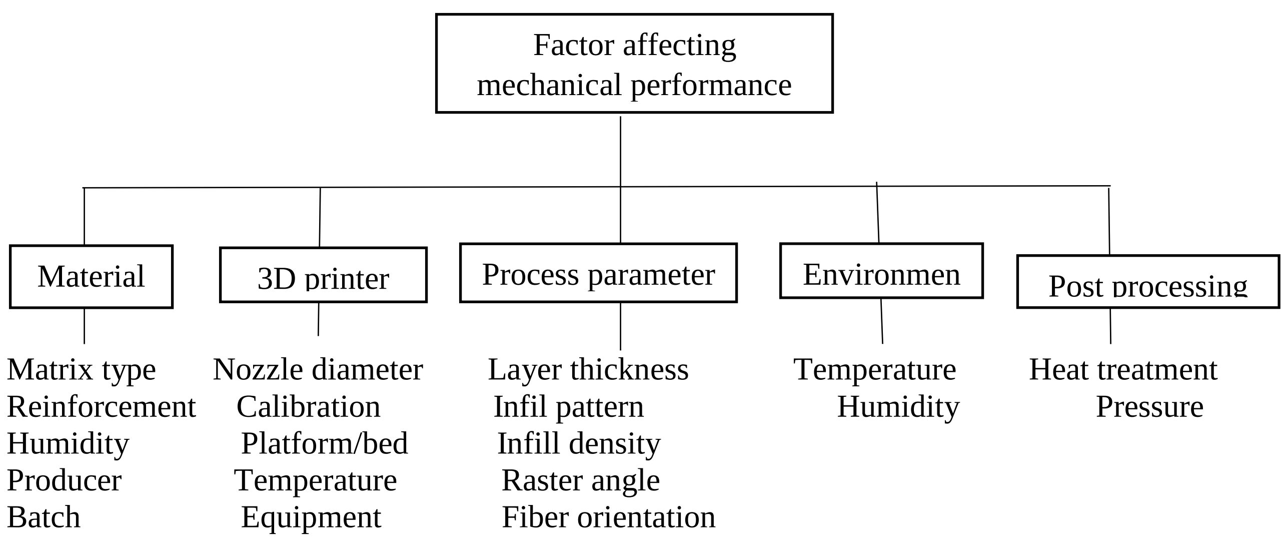

Figure 2-1: Factors influencing the mechanical performance of the 3D printed specimen (Sanei & Popescu, 2020)

2.2.1 Effect of layer height and fiber orientation on mechanical property

Tymrak et al., (2014) examined how the orientation of deposition and layer height correlate with tensile strength, strain at tensile strength, and modulus. Acrylonitrile butadiene styrene fabricated using open source 3d printer. Results showed that specimens printed with a layer height of 0.2 mm exhibited the highest tensile strength, whereas those with a 0.4 mm layer height showed the highest elastic modulus. Among the orientations tested ($+45^0/-45^0$ and $0^0/90^0$), $+45^0/-45^0$ demonstrate greater strength, while $0^0/90^0$ had a higher elastic modulus. Rankouhi et al., (2016)concluded that the layer thickness and raster orientation should be as low as possible to improve the mechanical strength and the small airgap to material ratio is the main factor contributing to higher strength. Therefore, a minimum layer thickness produces higher tensile strength and elastic modulus due to smaller fusing gaps between the thermal interlayers.

Todoroki et al., (2020) explored the tensile properties of 3D orientation continuous carbon fiber-reinforced thermoplastic composites in various directions. They conducted tensile tests and observed that eliminating the starting point of fiber bundles reduced scatter in 0°-tensile tests. However, the elastic modulus could increase during tensile loading due to fiber bundle curvature. Serpentine folded fiber bundles enhanced strength and stiffness in 90°-tensile tests, while their removal yielded appropriate results. In ±45°-tensile tests, folded fiber bundles led to lower shear strength, and their removal caused significant plastic deformation and rotation of fiber bundles, complicating shear strength measurements. Additionally, in lay-up direction tests, stiffness decreased by 40% compared to 90°-tensile tests, and strength dropped by 25%.

Papa et al., (2021) studied how fiber orientation affects the mechanical properties of novel composites and assessed how it impacts surface quality. They used Onyx, a carbon nanofiber material, as the matrix, which is a blend of carbon polyamide and short carbon fibers, with carbon fiber as the reinforcement. The results showed that specimens with 0^0-degree reinforcement had significantly improved tensile strength compared to matrix-only ones, while those with $0^0/90^0$-degree reinforcement did not show significant tensile strength improvements. The surface analysis confirmed that the orientation specimens' finish quality was suboptimal and strongly influenced by material and printing settings.

2.2.2 Effect of infill density and raster angel on mechanical property

Naima Khalid et al., (2021) reviewed on the mechanical characteristics of polyamide-reinforced carbon fiber (PACF) composites used in 3D printing. They examined how printing parameters during manufacturing influenced interlayer bonding and subsequently affected the mechanical properties of the samples. The study revealed a significant correlation between orientation, interlayer bonding, and tensile properties, with continuous fibers oriented at 0° raster angle notably enhancing the load-bearing capacity of the composites. The 0° orientation exhibited higher tensile strength parallel to the deposition direction and greater energy absorption in flexural strength compared to other angles. Polyamide-reinforced carbon fiber bonding at a 0° angle demonstrated superior mechanical properties when compared to raster angles of 45° and 90°.

Al Rashid et al., (2022) investigated the influence of different infill patterns and densities on the mechanical characteristics of 3D-orientation carbon fiber-reinforced PA6 composites was also examined. It was found that both infill patterns and densities had a notable impact on the mechanical properties of the 3D-orientation composites, with higher infill densities resulting in higher failure loads across all infill patterns.

Gao et al., (2023)investigated the effects of infill density and reinforced perimeters on continuous carbon fiber-short fiber synergistic reinforced composites. They observed that a higher density of reinforced perimeters led to a higher tensile modulus, indicating superior tensile properties in composites with more reinforced perimeters compared to those with fewer reinforcements.

2.2.3 Impact of carbon fiber reinforcement

Hao et al., (2018) researched on creating continuous carbon-fiber reinforced thermosetting composites through 3D printing and subsequently assessed their mechanical properties. The findings indicated that the mechanical performance of these 3D orientation thermosetting composites surpassed that of comparable 3D orientation thermoplastic composites and 3D orientation short carbon fiber reinforced composites.

Dul et al., (2021) conducted a comparative study on the impact of carbon fiber reinforcement in PA between 3D orientation and compression-molded samples. They also analyzed the effects of two different build orientations in 3D printing, namely XY and Z. The test results indicated that the elastic modulus and strength of 3D-orientation samples were slightly lower than those of compression-molded samples. Specifically, the tensile performance showed a 34% increase in tensile strength and a 147% increase in tensile stiffness compared to neat PA. Regarding flexural behavior, PA/CF-XY samples exhibited an average increase in flexural strength and stiffness by 29% and 140%, respectively. However, the fracture toughness of 3D-orientation PA/CF composites was higher than that of neat PA samples in both XY and Z build orientations.

Hendlmeier et al., (2021) studied comparison between 3d orientation carbon fiber reinforced PA6 and compression molded carbon fiber reinforced PA6. Three different filling patterns were used 0^0, $\pm45^0$, and 90^0 while the shell remained the same. The carbon content per weight was determined using Thermogravimetric analysis and should be below 20 wt/wt%. for the AM samples, the 0^0filament deposition performs the best, consistent samples, the fibers reinforce the material, and the samples do not undergo matrix-dominated failure and are comparable to samples made from the same material stock via compression molding. The $\pm45^0$ outperforms the 90^0 in both Young's modulus and tensile strength. Table 2-1 shows mechanical property comparison between pure PA6 and PA6 reinforced with carbon fiber.

Table 2-1: Mechanical property comparison between CFRPA6 and PA6 (Hendlmeier et al.,2021)

Items	Pure PA6	CF(mass ratio)			
		5	10	20	30
Tensile strength/ MPa	72	95	125	155	176
Elastic Modulus/MPa	3100	6035	8025	10075	12355
Flexural strength/MPa	110	145	170	185	205
Flexural Modulus/MPa	2500	4565	8700	10145	13455
Rockwell Hardness	95	98	105	115	118
Impact Hardness/KJ/m^2	Did not break	Did not break	45	28	25

Lupone et al., (2022) examined carbon fiber-reinforced Nylon composites with varying fiber concentrations, estimating the elastic modulus using a composite volume-average approach. Their findings highlighted the positive impact of carbon fiber on mechanical properties, with the elastic modulus closely matching predictions for low fiber content but deviating significantly for high fiber content due to increased porosity.

Pejkowski et al., (2023) examined the mechanical performance of 3D-orientation polyamide and reinforced polyamide materials. The reinforced filaments included PA12 filled with glass bubbles and PA12 filled with short carbon fibers. The test results revealed a reduction in tensile strength: PA12 decreased by approximately 24%, PA12BG (glass bubbles reinforced) by 21%, PA12CF-AM (carbon fiber reinforced) by 33%, and PA12CF (carbon fiber reinforced) by 31%. The material that exhibited higher tensile strength, tensile modulus, and creep resistance was the one where the carbon fibers broke before pull-out.

2.2.4 Effect of printing parameters on CFRP

To assess the mechanical characteristics of 3D-orientation components and the variations in these characteristics when employing various user-controlled printing and slicing parameters. Continuous fibers, along with short fibers, enhance the mechanical characteristics of 3D-orientation composites. However, continuous fiber composite orientation in 3D exhibits significantly greater strength compared to composites with short fibers (Zeeshan et al., 2023).

Botelho et al., (2003) compared the mechanical properties of carbon fiber-reinforced polyamide composites using interfacial polymerization and hot compression molding techniques. They investigated two types of matrices, polyamide 6 and polyamide 6/6, with fabric and unidirectional carbon fiber reinforcement. The results indicated a slight enhancement in elastic modulus, tensile strength, and compressive strength with increasing carbon fiber content. Interestingly, higher carbon fiber content in polyamide 6/6 composites led to increased shear compression values, whereas in polyamide 6 composites, the interlaminar shear strength remained unaffected by carbon fiber volume fraction.

Peng et al., (2020) studied how processing parameters affect the tensile performance of FDM-orientation carbon fiber-reinforced polyamide 6 (CF/PA6) composites. They investigated the impact of these parameters on both macroscopic performance and microstructure of the CF/PA6 filaments they fabricated. The focus was on understanding how temperature control improves interlayer adhesion. They used CF/PA6 filaments with a diameter of 1.75 mm, extruded from prepared pellets using a desktop single-screw filament extruder with a screw speed of 30 rpm. The extruder barrel was heated to 240°C, and the die temperature was 250°C. After extrusion, the filaments were cooled in a 0.5 m long water bath at around 40°C and wound by a winding unit. The FDM-orientation specimens had infill support, with an overlap area of 12.5 × 25 mm^2. The CF/PA6 honeycomb structure displayed excellent energy absorption and rebound behavior, indicating promising applications in complex industrial parts.

Le Gentil et al., (2023) conducted a study to analyze energy consumption and mechanical performance data to find the optimal solution for a particular requirement. They conducted experimental tests using CarbonX™ NYLON 6 + CF GEN 3 filament with a carbon fiber content of less than 20% by weight. Five printing parameters were chosen: bed temperature, nozzle temperature, layer thickness, deposition speed, and bed heating strategy. The results showed that the bed heating strategy and layer thickness were the primary factors influencing both energy consumption and ultimate tensile strength (UTS).

2.3 Tribological property of CFRP

Tribology is the study of objects in motion relative to each other, encompassing the physical phenomena related to contact mechanics, friction, lubrication, and wear (Popov & Psakhie, 2007). "Tribo" originates from Greek and signifies rubbing, making it essentially the study of friction between distinct surfaces moving at varying speeds (Bhadauria et al., 2019). Tribology involves the examination of how surfaces interact when they move against each other, focusing on factors like friction, wear, and lubrication. This field is essential across industries like mechanical engineering and manufacturing, as it directly impacts the efficiency and longevity of mechanical systems. Tribological aspects include characteristics such as friction coefficient, wear speed, surface texture, effectiveness of lubricants, and the hardness of materials. Optimizing these properties is key to designing and maintaining machinery for optimal performance.

2.3.1 Wear

Wear on material surfaces is a frequent occurrence characterized by gradual erosion or displacement, typically caused by the interaction of solid surfaces as they rub, slide, mesh, or grind against each other upon contact (Ajuka et al., 2023). 3D-orientation polymers demonstrate reduced friction and wear because of a larger contact area, plastic deformation, and the breaking of surface irregularities in certain sliding scenarios (Norani et al., 2021).

Stages of Wear

Under normal operating conditions, property changes during usage typically occur in three distinct stages:

- Primary or early stage (run-in period): The rate of change is often high during this initial phase.
- Secondary or mid-age stag: A steady rate of aging is maintained, encompassing most of the component's useful or working life.
- Tertiary or old-age stage: The aging rate accelerates significantly, leading to rapid failure (Prabhu et al., 2014).

Wear phenomena can be categorized into various types based on the nature of the tribological forces and the materials in question. Examples include sliding wear, fretting wear, abrasive wear, and material cavitation. Several mechanisms contribute to wear, with the following four being particularly significant.

- Surface fatigue
- Abrasion
- Adhesion
- Tribochemical reaction

2.3.1.1 Abrasive wear

Abrasive wear occurs when a solid object comes into contact with particles of a material that are of equal or greater hardness. A typical example of this issue is the wear experienced by shovels used in earth-moving equipment. The impact of abrasive wear is often underestimated, as any material, regardless of its overall softness, can cause abrasive wear when it contains hard particles.

The abrasive wear rate in a specific wear regime is typically inversely related to the hardness of the material being worn, directly related to the applied load, and influenced by the sliding speed, assuming thermal effects are negligible (Binder et al., 2017). The hardness of abrasive particles significantly affects the abrasion rate of the material being worn. When the abrasive particles are harder than the material, the rate of abrasive wear usually increases. This is because harder abrasive particles can penetrate the surface and remove material without their cutting edges becoming damaged or rounded.

Abrasive wear can be categorized into two fundamental modes:

- Two-body abrasive wear: this type of wear occurs when hard particles or grits physically remove material from the opposing surface. This resembles a cutting or plowing action, where the material is either displaced or cut away.
- Three-body wear: in this mode, particles are not confined and can freely roll and slide along a surface. Wear is categorized as open or closed depending on the contact condition. An open contact situation implies that surfaces have moved apart enough to act independently.

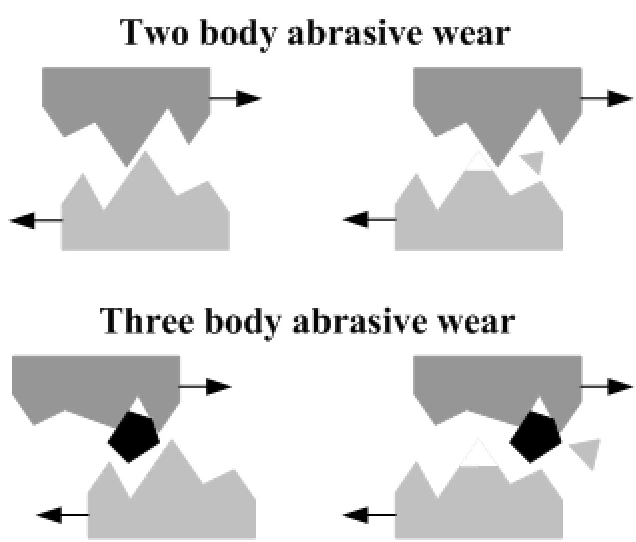

Figure 2-2: Two-body and three-body abrasive wear (Binder et al., 2017).

2.3.1.2 Adhesive wear

Adhesive wear typically happens when materials of similar hardness slide against each other, especially when there's a strong adhesive force at play. As they slide, certain surface irregularities experience significant plastic deformation and form weld-like connections (Aghababaei et al., 2016).

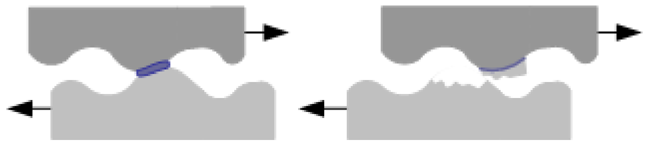

Figure 2-3: Adhesive wear (Aghababaei et al., 2016).

2.3.2 Effect of printing parameters on wear

Kumar et al., (2021) studied the wear characteristics of materials fabricated through additive manufacturing. They employed a pin-on-disc setup to assess the wear rate, utilizing parameters such as a load of 50N, a speed of 100 RPM, a test duration of 10 minutes, and a track diameter of 50 mm. The study focused on dry sliding tests performed at various part orientations (0, 45, 60, 90°). Results showed the highest wear rate of 1300 mm for polylactic acid (PLA) at a 90° orientation and 2300 mm for acrylonitrile butadiene styrene (ABS) also at a 90° orientation. Hanon et al., (2020) studied how the FDM 3D-printing process impacts the friction and wear performance of HT-PLA polymer test pieces. It was found that test pieces oriented in the X direction exhibited the most favorable friction and wear characteristics. Conversely, pieces oriented in the Z direction showed higher dynamic friction values compared to those in the X direction.

Naik et al., (2022) investigated the influence of fiber orientation and applied load on the wear properties of additively manufactured composite specimens using continuous carbon fiber as reinforcement and onyx (a blend of chopped carbon fiber and nylon) as the matrix material. Optical microscopy was employed for morphological analysis of worn surfaces, while wear properties were assessed using pin-on-disk equipment. The study found that wear and friction coefficient increased with higher fiber orientation angles and loads, with the least impact observed at 0^0 fiber orientation and the most significant at 90^0 fiber orientation. The worn surface analysis highlighted reasons for matrix failure and fiber fracture at different orientations: 0^0 orientation showed maximum wear thinning of fibers, resulting in minimal wear; 45^0 orientation exhibited some fiber debonding and wear thinning; and 90^0 orientation led to maximum fiber fracture and wear.

Chhabra et al., (2023) examined how key process parameters such as layer height, build orientation, wall line width, and wall thickness can enhance the wear resistance of PA12CF20 using GA-ANFIS (Genetic Algorithm-Adaptive Neuro-Fuzzy Inference System). The test specimens were produced according to ASTM G99 standards, and a pin-on-disk wear testing machine was employed for sliding wear tests. The results indicated that wear rates were initially high but decreased as the wear line approached a straight line. The minimum wear rate achieved was 0.000348184 mm3/m under optimized conditions, including a layer thickness of 0.12 mm, build orientation of 0^0, wall line width of 0.35 mm, and wall thickness of 0.80 mm.

2.3.3 Effect of carbon fiber content on wear

In recent times, the advancement of carbon fiber-reinforced materials has been rapid, leading to composite materials that combine the best features of both components. These enhancements include greater hardness and rigidity compared to pure nylon, reduced susceptibility to high-temperature deformation, substantially improved thermal stability, increased resistance to abrasion, outstanding fire resistance, and more (Zhang et al., 2012). The effect of carbon fiber content on the tribological performance of CF/Polyimide composites sliding at various temperatures was investigated by (Dong et al., 2018), followed by determining an appropriate filler ratio. The composites were produced with carbon fiber volumes 0%, 5%, 10%, 20%, and 30% using hot pressing. Results showed that adding carbon fiber improved flexural and tensile properties, dynamic mechanical properties, and wear resistance of polyimide, especially at higher temperatures. The composite with 20vol% carbon fiber exhibited the lowest friction coefficients (0.054 at 180°C and 0.1 at 260°C) and lowest wear rates.

Cai & Wang, (2012) studied the impact of carbon fiber content on the friction and wear performance of PA6 composite. They conducted friction and wear tests at 0.42 m/s for 1 hour under loads 10, 20, 30,40, 50, 60, 70, 80, and 90 N using a block-on-ring wear tester and examined the worn surface with a scanning electron microscope. The results showed that adding carbon fiber improved the wear resistance of polyamide 6, with an optimal carbon content of about 5 vol.%. The wear of the PA6/Carbon fiber composite was lower than that of pure PA6, with a gradual increase in wear as load increased while the friction coefficient decreased. However, the composite's friction coefficient was slightly higher than that of pure polyamide 6. Li & Xia, (2009) investigated the impact of carbon fiber reinforcement on the tribological behavior of polyamide under dry sliding conditions. They used varying compositions of carbon fibers as reinforcement and analyzed the worn material's surface morphology using SEM. The study tested both filled and unfilled polyamide composites using a CGr15 ball. Results indicated that the optimum wear resistance was achieved with a 20 vol% carbon fiber content. As load and sliding frequency increased, the friction coefficient and volumetric wear of both neat PA6 and CF/PA6 composites decreased. The addition of carbon fiber significantly reduced the primary wear mechanisms of adhesion and plastic deformation observed in pristine PA6 under dry sliding conditions.

Unal & Mimaroglu, (2012) analyzed the friction and wear behavior of different polyamide-6 (PA-6) composites, including graphite-filled PA-6 at 5 wt% and 15 wt%, as well as 4 wt% wax-filled PA-6 (PA-6+4% wax), sliding against stainless steel under dry conditions using a pin-on-disc tribometer. It explored how the type and amount of filler, applied load, and sliding speed affected their tribological properties. Tests were conducted at sliding speeds of 0.4 m/s, 0.8 m/s, and 1.6 m/s, with applied loads of 50 N, 75 N, and 100 N. Scanning electron microscopy (SEM) was used to examine the microstructure of worn surfaces and the wear mechanisms. The study found that the wear rate was significantly influenced by sliding speed but had minimal impact from changes in applied load. Among the materials studied, the lowest wear rate observed was 6.910-15 m2/N for the 4 wt% wax-filled PA-6 composite, while the highest rate was 2.12x10-14 m2/N for pure polyamide-6.

Zhou et al., (2013) analyzed how adding carbon fiber affects the structure, mechanical, and tribological properties of PA6/PPS composites, offering practical guidance for using polymer-based composites. Carbon fiber reinforcement improved the strength, modulus, and hardness of PA6/PPS composites, although it reduced the breaking elongation rate and impact strength to some extent. During friction tests, the friction coefficient of PA6/PPS composites initially increased rapidly before stabilizing, with the stabilized friction coefficient of PA6/PPS-CF composites lower than pure PA6/PPS blends. Increasing carbon fiber content led to higher wear rates in PA6/PPS-CF composites. Under high load or speed, friction coefficient decreased and wear rate increased, but under relatively high load or speed conditions, wear resistance improved in PA6/PPS-CF composites. SEM of worn surfaces revealed adhesive wear as the main wear mechanism in PA/PPS-CF composites.

Gadelmoula & Aldahash, (2023) the studies compare the friction and wear behavior of carbon fiber-reinforced polyamide 12 (CF-PA12) with pure polyamide 12 (PA12). Test specimens were created using selective laser sintering (SLS) at five different build orientations and tested using a pin-on-disc tribometer under dry sliding conditions. Measurements included the coefficient of friction (COF), interface temperature, friction-induced noise, and specific wear rate. Scanning electron microscopy (SEM) was used to analyze the tribo-surfaces. The findings showed that both the COF and contact temperature of CF-PA12 are independent of orientation and lower than those of pure PA12. Additionally, CF-PA12 exhibited a 25% lower COF and 15–40% higher wear resistance compared to pure PA12. SEM analysis revealed that adhesive wear was predominant on the surface of pure PA12, while both adhesive and abrasive wear patterns were present in CF-PA12. Furthermore, fiber crushing and thinning were observed, which could significantly increase frictional noise under certain conditions.

2.4 Additive Manufacturing Fabrication Process

AM technology can be categorized into two primary dimensions. The first dimension pertains to the material type utilized, which can range from solid, liquid, to powder forms. The second dimension relates to the deposition technique employed for fabricating parts. Each of these processes possesses unique capabilities, constraints, and utility across various applications, particularly in constructing prototype models. Presently, there exists a variety of AM processes in the market, distinguished by specialized sintering, layering, or deposition methodologies.

2.4.1 Selective laser sintering

The Selective Laser Sintering (SLS) process, which originated at the University of Texas at Austin in 1986 and was later commercialized by DTM Corporation, has gained popularity for several reasons (Gan et al., 2020). One key advantage is that SLS can fabricate parts without the need for support structures and offers versatility in using various powder materials. These materials include polycarbonate (PC), nylon, nylon/glass composites, wax, ceramics, true form (TM), elastomeric substances, and metal-polymer powders (Singh et al., 2012). In the SLS process, solid parts are created by fusing powdered materials using a CO2 laser beam as shown in Figure 2-4. A thin layer of powder is spread over the build surface and preheated just below its melting point. The laser beam then selectively sinters and bonds the powder in a cross-sectional pattern to form a layer of the part. This process is repeated with successive layers of powder until the entire part is constructed (Negi et al., 2013). The advantages of SLS include its ability to work with a variety of thermoplastic powders, ease of post-processing, and the absence of a need for support structures. However, drawbacks include the potentially abrasive surface of the sintered models and the relatively high costs associated with this method (Gueche et al., 2021).

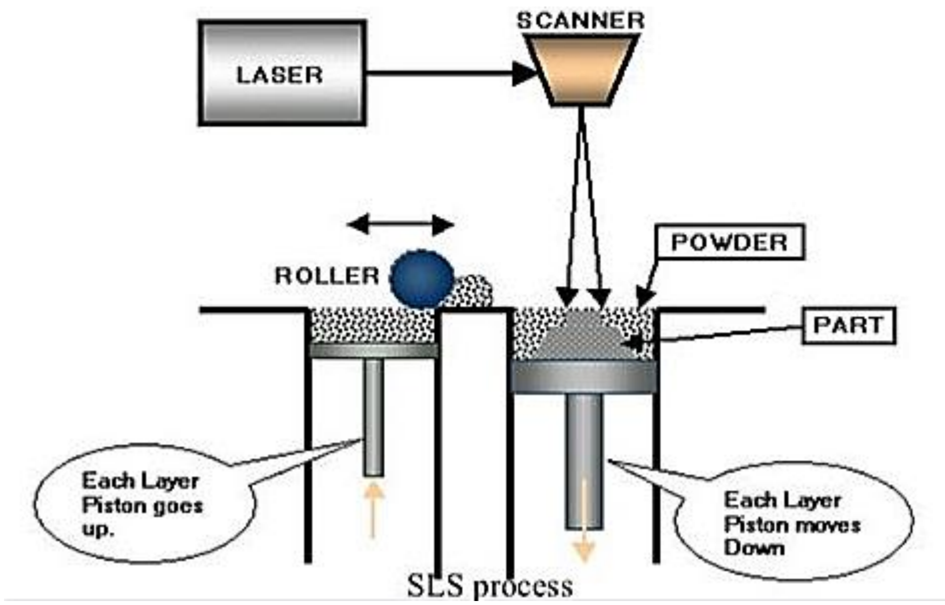

Figure 2-4: Selective laser sintering process (Gan et al., 2020)

2.4.2 Fused filament fabrication process

Fused deposition modeling (FDM) stands as one of the most frequently utilized technologies in 3D printing (additive manufacturing). This approach is also prevalent in various additive manufacturing methods, including additive layer manufacturing, layered manufacturing, additive fabrication, additive techniques, additive processes, and solid freeform fabrication. Among these methods, fused filament fabrication (FFF) stands out as the most widely used process in additive manufacturing. First, computer-aided design (CAD) software is utilized to create a 3D model, which is then saved in the stereolithography (STL) file format. Subsequently, the STL file is employed in the layer-by-layer fabrication process, typically by directly uploading it to the corresponding software of the manufacturing machine (Chhabra et al., 2023; Norani et al., 2021). As shown in the Figure 2-5 in (FFF), the process begins with introducing a material filament into a machine using a pinch roller mechanism, where it melts within a heated liquefier, utilizing the solid part as a piston to propel the melt through a print nozzle. The extruded semi-molten material is then deposited onto a heated bed in layers, guided by a gantry on the horizontal x-y plane, while the build surface adjusts vertically in the z-direction. As the material solidifies, it bonds with the surrounding material, enabling the creation of complex plastic parts. Simultaneously, the plastic filament is fed into a heated extruder via a motor-driven coil reel, transforming it into molten paste extruded from the nozzle tip, forming lines on the base plate based on pre-designed tool paths to create surfaces and eventually a 3D part. Each layer's completion involves lifting the extruder by a distance equal to the layer thickness for the next layer. Despite its ability to fabricate complex shapes, this layer-by-layer process is accompanied by drawbacks such as extended build times, diminished surface finish, and reduced mechanical strength (Jin et al., 2015; Tian et al., 2016).

Numerous parameters significantly influence the characteristics of the fabricated parts and their production efficiencies. Among the crucial factors are the infill density, build orientation, layer thickness, printing speed, raster angle, infill pattern, extrusion temperature, raster width, nozzle diameter, contour width, number of contours, contour-to-contour air gap, and air gap, among others (Solomon et al., 2020).

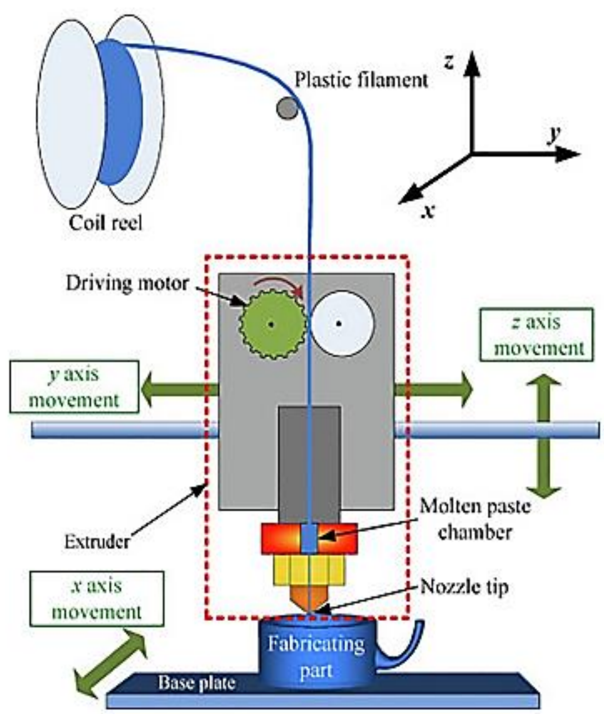

Figure 2-5: Fused filament fabrication process (Solomon et al., 2020)

2.5 Research Gap

Research on 3D printed materials is expanding, but most studies focus on print parameters' impact on mechanical properties, with little attention given to print orientation's influence on tribological properties, and there is a lack of research on optimizing wear parameters for 3D printed carbon fiber-reinforced polyamide. This research aims to address these gaps by investigating the impact of print orientation on both mechanical and tribological properties, and by optimizing wear parameters to enhance material performance in practical applications. To support this analysis, LS-DYNA simulations will be employed to evaluate stress and deformation of the material, providing comprehensive insights into the material's behavior under different wear test conditions.

CHAPTER THREE

MATERIALS AND METHODOLOGY

3.1 Introduction

This chapter details a research study on 3D-orientation CFRPA material properties, fabrication method, devices, equipment, experimental procedure, and testing setups, focusing on the effects of print orientation on wear, hardness, tensile strength, density, and porosity.

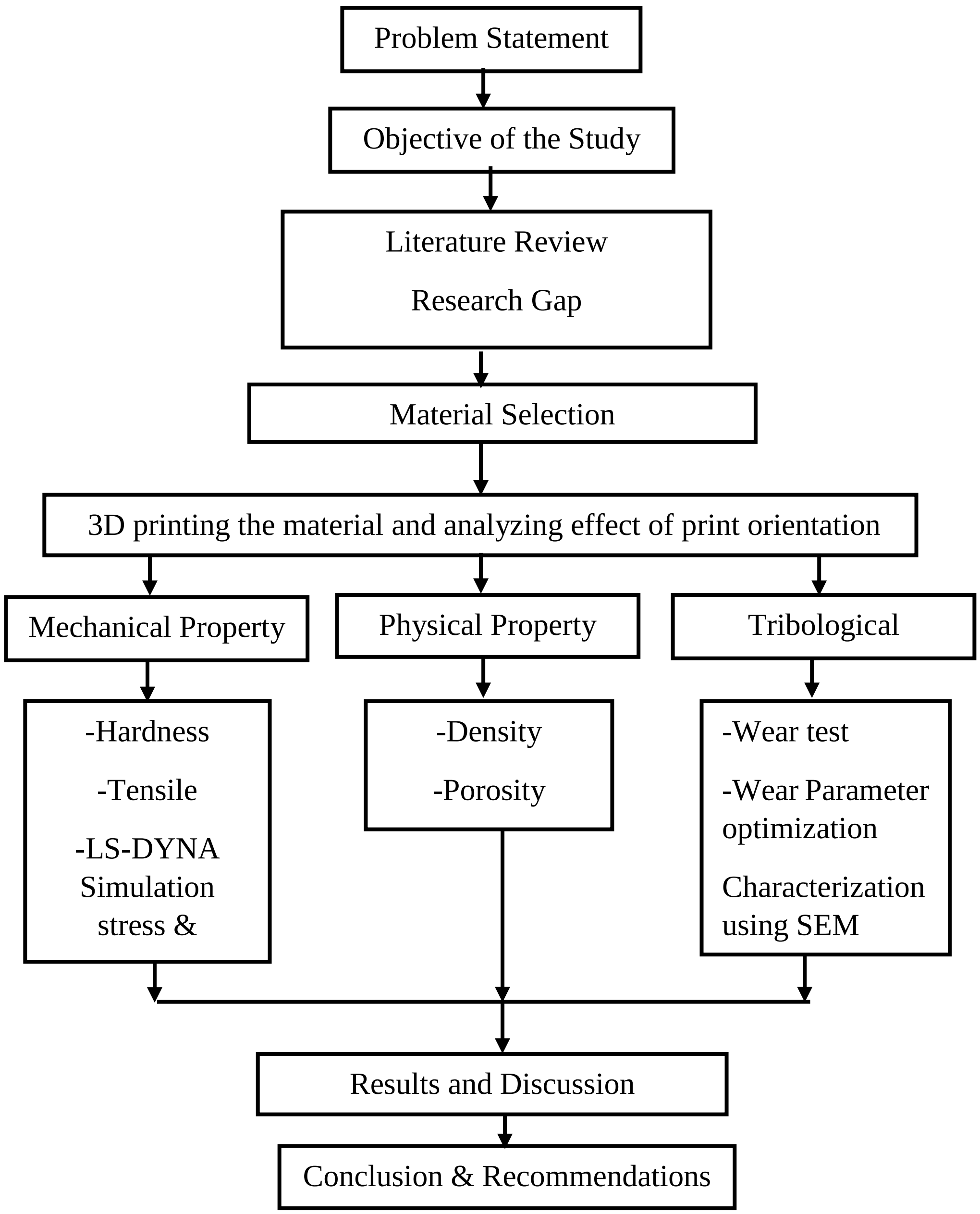

Figure 3-1: Flow chart of research method

3.2 Materials

The material selection process involved a thorough review of available polymer composites, focusing on those with carbon fiber reinforcement due to their favorable characteristics. The selection of material was driven by its superior mechanical properties and potential applications in various engineering fields. The material selected for investigation was a 3D orientation composite consisting of 15% carbon fiber-reinforced polyamide 6 (CF15%-PA6). CFRPA6 is known for its enhanced strength, stiffness, and thermal stability compared to unreinforced polyamide 6, making it a suitable candidate for high-performance components produced through additive manufacturing.

3.2.1 Polyamide

Polyamides are categorized as semi-crystalline polymers, meaning their molecular chains tend to organize into crystalline regions known as "crystallites" in the solid state. The orderly arrangement of these chains is maintained through interactions between the amino group of one chain and the carboxyl group of adjacent macromolecules (Venoor et al., 2021). Polyamide is valued for its exceptional strength, resilience, and elasticity, making it suitable for various commercial and industrial applications. Its high melting point, excellent wear resistance, and relatively low coefficient of friction also make it suitable for applications involving heat and friction. In 3D printing, polyamide is widely used due to its superior strength-to-weight ratio and ability to produce intricate shapes with high dimensional accuracy. It is commonly used to manufacture functional prototypes, final components, and a variety of consumer goods.

Table 3-1: Mechanical and physical property of polyamide (Gangaraju et al., 2023)

	Mechanical property of polyamide
Density Kg/m^3	1130
Melting temprature ^{0}c	223
Resistivity ohm*mm^2/m	1E+17
Friction coefficient	0.415
Tensile strength MPa	66.5
Young’s modulus MPa	2400

3.2.2 Carbon Fiber

Carbon fiber is a lightweight and exceptionally strong material comprising thin strands of carbon atoms known as carbon fibers. These fibers are produced by heating synthetic fibers or organic precursor materials like polyacrylonitrile (PAN), rayon, or petroleum pitch at high temperatures without oxygen, a process called carbonization or pyrolysis. This process eliminates non-carbon elements, forming long, tightly bonded carbon chains. Compared to traditional materials such as steel and aluminum, carbon fibers are significantly stronger and lighter, making them advantageous for applications where weight reduction and strength are crucial. They are extensively used in industries like aerospace, automotive, sports equipment, wind energy, marine, and civil engineering (Ahmad et al., 2020). Table 3-2 shows mechanical and physical property of carbon fiber

Table 3-2: Mechanical and physical properties of carbon fiber (Li & Xia, 2009)

Mechanical property	**Carbon fiber**
Density (kg/m^3)	1740
Linear density (mg/m)	56
Tensile strength (MPa)	2000
Linear resistance (Ʊ/m)	650
Diameter (μm)	7
Length (μm)	105

Figure 3-2: Carbon fiber reinforced polyamide 6 filament

3.3 Machines and Equipment

The following table lists the equipment and machines used in the research for investigating the effect of print orientation on the mechanical and tribological properties of CFRPA.

Table 3-3: Tools and equipment

S. No	Tools	Function
1	Roboze Plus PRO printer	To print the material
2	Minitab 21 software	Minitab is a software package used for the analysis of data and optimization of wear parameters
3	Weight balance	To measure the weight of samples
4	Pin on disk apparatus	To determine the wear rate of material
5	Universal testing machine	To determine the tensile strength of the material
6	Vickery hardness machine	To determine the hardness of composite
7	SEM	To characterize the worn surface
8	LS-DYNA software	To determine stress and deformation

3.4 Fabrication Process

The samples were produced using a Roboze Plus PRO printer, utilizing a filament with a diameter range of 1.75 ± 0.05 mm. This thermoplastic filament was then extruded through a nozzle with a diameter of 0.6 mm. To reduce moisture absorption by the filament from the atmosphere, the Roboze Carbon PA PRO spools underwent a drying cycle at 90°C for 12 hours in an HT Drye before initiating the printing process. The fabrication process of 3D orientation CFRPA6 using the Fused Filament Fabrication (FFF) process involves several key steps to ensure high-quality parts with specified parameters. The material used is CF15% PA6, a filament comprising 15% carbon fiber-reinforced polyamide 6. The 3D model of the part was created using solid work and imported into slicing software, where the print settings are adjusted the model is sliced to generate the G-code for the printer.

The printing parameters for the following data are:

- Chamber Temperature = 90 °C
- Extrusion Temperature = 270 °C
- Printing speed = 3600 mm/min
- Layer height = 0.2 mm
- Infill percentage = 100%
- Fiber orientation = 0^0

The printing process is conducted in three orientations: horizontal, vertical, and 45 degrees. For the horizontal orientation, the model is positioned on the print bed to ensure layers are deposited horizontally. The print job is started, with careful monitoring of the initial layers to ensure proper adhesion to the build plate. The process is repeated for the vertical orientation by reorienting the model in the slicing software and adjusting the print bed positioning accordingly. Finally, for the 45-degree orientation, the model is adjusted in the slicing software to be oriented at a 45-degree angle relative to the print bed, and the print job is started with similar monitoring.

3.5 Mechanical, Physical, and Tribological Tests

3.5.1 Hardness test

The hardness of material usually implies its resistance to deformation. These properties can vary based on the printing orientation due to the anisotropic introduced during the 3D printing. Hardness testing ensures the quality and consistency of the orientation parts. By comparing the hardness values for different printing orientations, manufacturers can identify variations and make necessary adjustments to the printing process to achieve uniform quality. Figure 3-4 shows the Vickers hardness testing machine. The Vickers hardness tester was employed, with a square-base diamond pyramid as the indenter. a diamond indenter is pressed into the surface of the material with a known force, usually in the range of 1 to 120 kilograms-force (kg). This combined angle between the pyramid's opposing faces is 136°. The load divided by the surface area of the indentation yields the diamond-pyramid hardness number (DPH), sometimes known as the Vickers hardness number (VHN or VPH). The Vickers hardness test uses a diamond indenter and a light force to create an indentation on the subject being tested. The depth of indentation is transformed into the hardness value of the object.

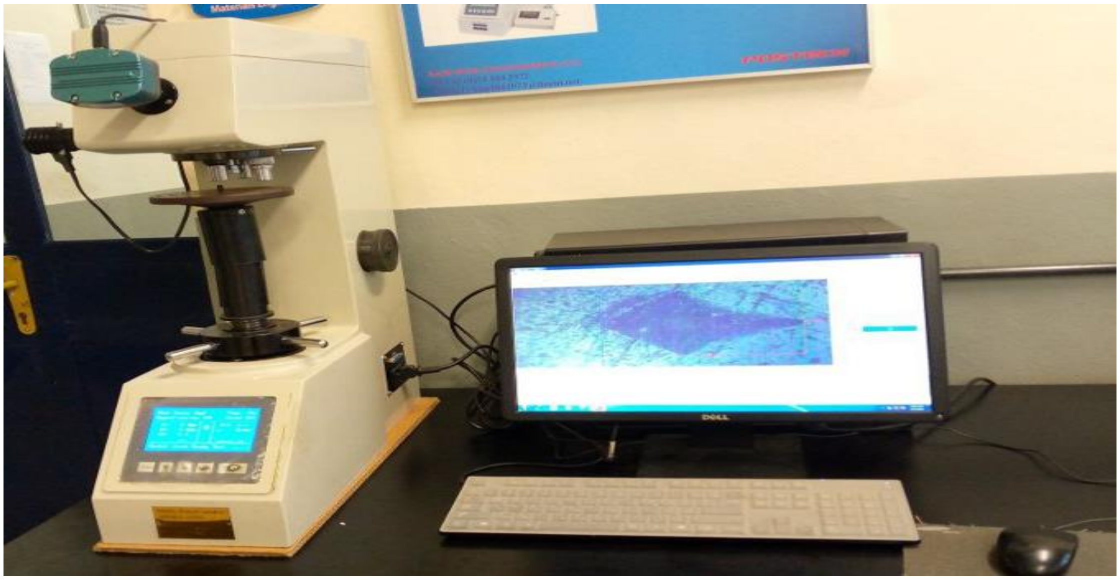

Figure 3-3: Vickers hardness test machine

3.5.2 Tensile Strength Test

Tensile strength testing provides critical data on the material's ability to withstand pulling forces. Since 3D printing can create anisotropic materials, the tensile strength can vary significantly depending on the print orientation (horizontal, vertical, and 45 degrees). UTM machine (Figure 3-5a) used for tensile strength testing. The standard ASTM for tensile testing of materials is ASTM D638 as shown in Figure 3-5b**.** The machine will pull the specimen until failure, automatically recording the necessary data. After the specimen breaks the UTM software will display the test results, including the maximum load and elongation.

$$Stress = \frac{Force}{Area} \tag{3.1}$$

$$Area = w * t \tag{3.2}$$

$$Strain = \frac{\Delta L}{L_o} \tag{3.3}$$

Where: w width, t thickness, L_o original length and ΔL the difference between elongated length and original length

(a) (b)

Figure 3-4: (a) UTM machine (b) sample prepared for tensile strength test

3.5.3 Density and porosity measurement

Measuring density helps ensure that the material composition and printing process are consistent, while porosity assessment identifies voids and defects that could weaken the material. Figure 3-6 (a) shows measuring of the weight of the sample in air and (b) shows measuring the weight of immersed the sample in distilled water to measure the buoyant force acting on the sample. This force is caused by the displaced water pushing upwards on the object, partially counteracting the force of gravity.

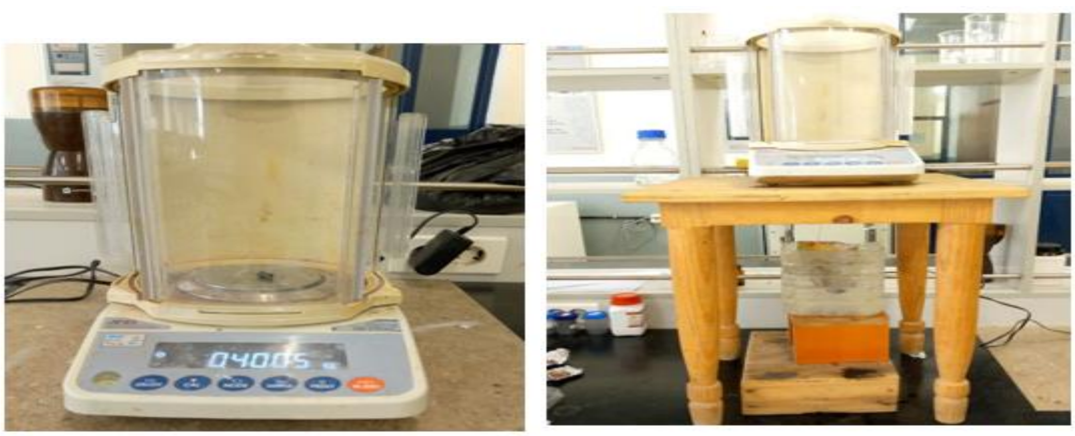

(a) (b)

Figure 3-5 (a) weight in air (b) suspended weight

The experimental density of horizontal, vertical and 45-degree orientation was calculated by dividing the measured weight of a test sample

$$\rho_{theo} = (\rho_{mat} * V_{mat}) + (\rho_{rein} * V_{rein}) \tag{3.4}$$

Where, V_{mat} and V_{rein} represent volume fraction of matrix and reinforcement respectively. ρ_{theo}, ρ_{mat} and ρ_{rein} represent the theoretical density of composite, density of matrix, and density of reinforcement respectively.

Actual or experimental density for the horizontal, vertical and 45degree orientation CFRPA6 was calculated as stated by Archimedes principles. (W air and then weighted in the distilled water (W water) by suspending samples in it. The actual density or experimental density of the 3D printed sample was calculated by the equation:

$$\rho_{actual} = \frac{m_{air}}{m_{air} - m_{water}} * \rho \tag{3.5}$$

Where, m air = mass of composite in air and m water = mass of composite in distilled water, and ρ = density of distilled water at 25 ^{0}C 1g/cm^{3}

the porosity of all samples was calculated by Eq. (3.6)

$$p = 1 - \frac{\rho_{act}}{\rho_{theo}} \tag{3.6}$$

Where P = the porosity of composite material, ρ_{actual} = the actual density of composite material, and ρ_{theo} = the theoretic density of composite material.

3.5.4 Wear test

According to ASTM G99-95 standards, a Pin-on-disc wear measuring Machine Figure 3-6 (a) was utilized to examine Dry sliding wear characteristics of fabricated samples (Prajapati et al., 2020). Wear pins having the dimensions of Ø6 mm×12 mm in height were displayed in Figure 3-6 (c). An Electronic weighing system was utilized to measure the weight of pins. A polished and hardened disc formed by EN32 steel (58-60 HRC) was used to counter-face the CFRPA composites. The pin surface and the counter face then become cleaned with acetone intermittently. In this, the pin is stationary within the holder and the E32 steel disc is rotating with the proposed speed. After running through a specified distance, the pins were extracted. After every run, the disc has to be cleaned with acetone and dried. After the tests, pins were weighted to check weight loss due to wear. The wear test for the specimens was conducted under different applied loads, sliding speeds, and track diameters under a constant time of 10 minutes. 27 samples were prepared for wear test 9 samples for each orientation. The results obtained experimentally were optimized and validated with regression analysis. ANOVA and interaction plots were used to determine the wear behavior of 3D-orientation CFRPA and the obtained results were compared.

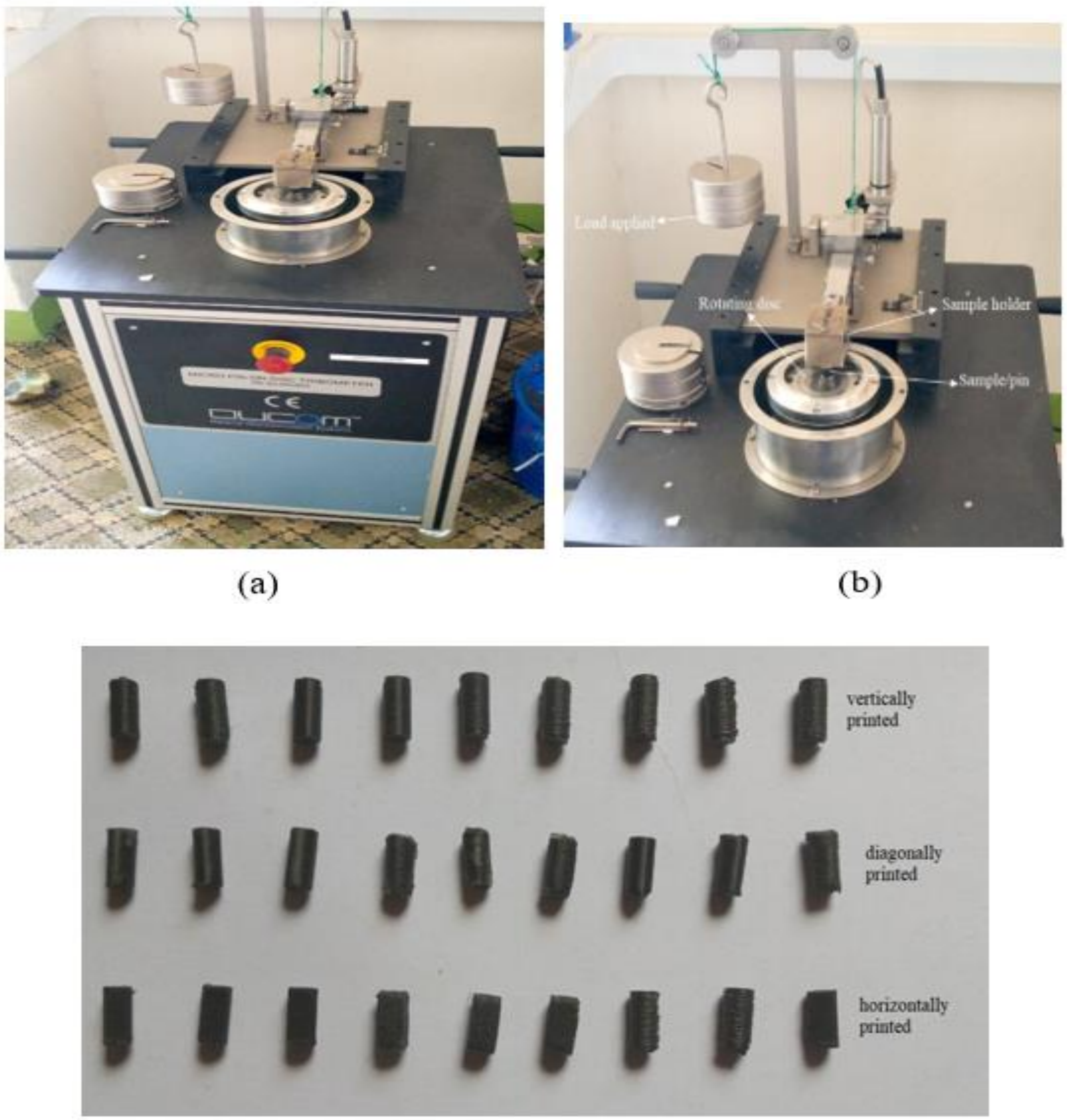

(a) (b)

(c)

Figure 3-6: (a) pin on disc machine (b) machine set up (c) samples prepared for wear test

The WR was determined as volume loss per unit distance of sliding. WR in dry sliding conditions, W in mm^3/m, may be expressed by rearranging the Archard's equation given in Eq. (3.10) . The WR of the sliding pin will be estimated by volume loss divided by distance of sliding. Weight loss of specimen is going to be determined by measuring the weight of the flathead pins after and before the tests (Liu et al., 2022).

- Determination of Weight loss

$$\text{weight loss} = m_b - m_a \qquad (3.7)$$

- Determination of wear volume (Odabas, 2018)

(Wear volume, w) (m^3) = weight loss (g) /density (g/mm^3)

$$WV = \frac{m_{loss}}{\rho} \qquad (3.8)$$

- Determination of sliding distance

$$SD = \frac{\pi * TD * SS * t}{60} \qquad (3.9)$$

- Determination of wear rate (WR) for all samples (Hanief & Charoo, 2021)

Wear rate (mm^3/mm) = Wear volume (mm^3) / Sliding distance (mm)

$$WR = \frac{v_w}{s_d} \qquad (3.10)$$

- Determination of wear coefficient

Wear coefficient = volume lost (mm^3) * surface Hardness (N/mm^2)/ Force(N) * total rotating distance(mm)

$$k = \frac{w * H}{F * St} \qquad (3.11)$$

- Determination of specific wear rate(SWR)

Specific wear rate (mm^2/N) = wear volume / load * sliding distance

$$SWR = \frac{WV}{F * SD} \qquad (3.12)$$

The average value of the weight loss percentage as a function of test time was calculated using the equation below. From weight loss of the specimens (Δm) it is possible to evaluate a dimensionless parameter known as w, "wear rate" define by Archard's equation (Shen et al., 2010).

$$W = \frac{\Delta m}{\rho . v . t . A} \qquad (3.13)$$

$$COF = \frac{F}{L} \tag{3.14}$$

Where: ρ = average density of a material, t = test time (s) and A = apparent contact area (mm^2), m_b= weight of a sample before wear, m_a= weight of the sample after wear

3.6 Selection of Process Parameters

The process parameters for the wear test were selected for the experiment based on the available literature. In Table 3-4 shows selected wear parameters by different researchers. Based on the literature review the process parameters were selected for the test as shown in Table 3-5.

Table 3-4: Wear parameters used by different researchers

Researchers	**Material**	**Tool used**	**Process parameters**
(Naik et al., 2022)	continuous carbon fiber-reinforced polymer (CFRP) composite material	Using pin on disc apparatus	Load (10, 20,30, 40,50) N Sliding speed (100rpm) Track diameter 50mm
(Prajapati et al., 2020)	CFRP composite	Using pin on disc apparatus	Load (50, 80, 110) N Sliding speed (300, 400, 500) rpm Sliding distance (500, 1000, 1500) m
(Chockalingam et al., 2022)	Nanocomposites of Polyethylene	Pin on disk	Load (10, 15, 20, 25) N Sliding distance (100, 200, 300, 400) m
(Unal & Mimaroglu, 2012)	wax polyamide 6 composites		Load (50,75, 100) N Sliding speed (0.4, 0.8, 1.6) m/s
(ÇOBAN & OKTAY, 2023)	CFRP composite	Ball-on-disc tribometer device	Load (1.3.5) N Sliding speed (0.02, 0.04) m/s Sliding distance (18-36) m

Table 3-5: wear test process parameters

Process parameters	First Level	Second Level	Third level
Load (N)	10	20	30
Sliding speed(rpm)	200	500	800
Track diameter (mm)	30	40	50

3.7 Methodology for Wear Optimization

3.7.1 Design of experiments

In this approach, the three-level three process parameter selected for experimental analysis is in Table 3-6. The optimum process parameters were preferred not only to improve quality but also in a way that they are less responsive to the testing conditions. Experiments were carried out according to the experimental plan based on the Taguchi L9 design:

Table 3-6: Experimental design matrix

S No:	Load (N)	Speed (rpm)	Track diameter(mm)
1	10	200	30
2	10	500	40
3	10	800	50
4	20	200	40
5	20	500	50
6	20	800	30
7	30	200	50
8	30	500	30
9	30	800	40

3.7.2 Taguchi-based grey relational analysis method

Taguchi Method is an approach for developing and carrying out experiments to investigate processes where the outcome depends on numerous parameters (variables; inputs) without having to laboriously and uneconomically run the process using all possible combinations of values for those variables. Grey relational analysis is extensively used to quantify the degree of interaction among sequences using grey relational grades. Several researchers have used grey relational analysis to optimize control parameters with multiple responses via grey relational grade (Jajimoggala et al., 2019). The integrated GRA integrates the Taguchi method's algorithms with grey relational analysis to determine the optimal value for process parameters with numerous performance criteria. The Taguchi method is used for optimization, but because it is a single response optimization strategy, it is applied together with grey relational methodology. Grey rational analysis reduces a multi-response to a single response, which is subsequently optimized using the Taguchi method.

3.7.3 Taguchi's orthogonal array

Taguchi's Orthogonal Array involves generating pairs of parameters from all levels at two-column intervals in the experimental table, ensuring that each composition appears with the same frequency (Krishna Vamsi et al., 2022). Orthogonal arrays balance experimental cost and precision by requiring fewer experiments to gather useful statistical data. However, these experiments are not full factorial, meaning some bias is inevitable. This bias is acceptable since not all composition levels are represented in the orthogonal array, which means the optimal composition might not be included in the experimental set.

3.7.4 Signal-Noise Ratio Analysis

To identify the optimum wear parameters, the Taguchi approach requires assessing the signal-to-noise ratio (S/N) of each extrusion parameter level for each output function. Analysis of the S/N ratio, that is, the lower-the-better, higher-the-better, and nominal the better, is the performance characteristic. Based on the S/N analysis, the S/N ratio for each level of process parameters is derived. Regardless of the performance characteristic category, the higher the S/N ratio, the better the performance characteristic (Sylajakumari et al., 2018). In Taguchi optimization, the S/N ratio represents a measure of quality features and is determined as follows

$$\frac{S}{N} = -10\log[\frac{1}{n}\sum_{i=1}^{n} Yi^2] \quad (3.15)$$

$$\frac{S}{N} = -10\log[\frac{1}{n}\sum_{i=1}^{n} \frac{1}{Yi^2}] \quad (3.16)$$

where Y = observation n = total number of observations, = the average of observed data, and Y = ith response. Eq. (3.15) is utilized for smaller better S/N ratios, and Eq. (3.16) is appropriate for greater better S/N ratios. To reduce wear rate, specific wear rate and COF the S/N ratio is estimated using the smaller-is-better criterion (Krishna Vamsi et al., 2022).

3.7.5 Analysis of variance (ANOVA)

The analysis of variance (ANOVA) was used to determine which parameters have a significant influence on the quality attribute. The statistical approach of ANOVA is used to determine the influence of all control values. The percentage contributions of each control factor are used to measure the associated impacts on the performance characteristics in the analysis of variance. This analysis used a significance level of 5%, corresponding to a 95% level of confidence. The ANOVA findings show whether or not there is a statistically significant variation in output characteristics. ANOVA analysis is used when values are less than 0.05 and more than 0.05 are not significant.

3.7.6 Optimization steps used in grey relational analysis

Step 1: Depending on the type of quality feature, convert the original response data into S/N ratio (Yij) using the relevant formula stated in Eq (3.15 and 3.10).

Step 2: In this stage, the measured quality characteristics, such as wear rate and coefficient of friction, are initially normalized to a range between zero and one. This procedure is referred to as Grey relational generation. Three methods are employed for normalization. If the original sequence's target value is infinite, it is characterized as "the-larger-the-better." To prevent the effect of using various units and to reduce variability, normalize Yij as Zij (0 _ Zij _ 1) using the following formula. Normalization is a transformation done on a single input to uniformly distribute and scale the data into an acceptable range. Zij denotes the normalized value for the ith experiment/trial and the jth dependent variable/response.

$$Zij = \frac{Yij - Ymin}{Ymax - Ymin} \quad (3.17)$$

$$Zij = \frac{Ymax - Yij}{Ymax - Ymin} \quad (3.18)$$

When the original sequence's larger-the-better characteristic is considered, the original sequence should be normalized using Eq. (3.17). When the original sequence's smaller-the-better characteristic is considered, the original sequence should be normalized using equation (3.18) (Muthu, 2020).

Step 3: Compute the grey relational coefficient (GRC) for the normalized S/N ratio values

$$GRCij = \frac{\Delta min + \partial \Delta max}{\Delta ij + \partial \Delta max} \quad (3.19)$$

Where, i= 1, 2, ..., n-experiments and j== 1, 2, ..., m-responses GRCij = GRC for the ith experiment/trial and = absolute difference between Yoj and Yij, min = minimum value of and max = maximum value of is the distinguishing coefficient which is defined in the range 0 1 Step Yoj = optimum performance value or the ideal normalized value of jth response Yij = the ith normalized value of the jth response/dependent variable

Step 4: Compute the grey relational grade (GRGi).

$$GRGi = \frac{1}{m} \sum GRCi \quad (3.20)$$

where m is the number of responses. Step 5: Select optimal levels for the factors based on the maximum average GRGi value using the response graph method or ANOVA.

3.8 Simulation using LS DYNA

LS-DYNA is a dynamic finite element software renowned for its transient analysis capabilities. It is often employed to examine structures experiencing substantial deformations using explicit time integration methods. This software excels at addressing complex nonlinear dynamic problems due to its extensive material resources. Users can either utilize the diverse material options from the built-in library or create custom material models, enabling precise definitions of element properties and structural behavior. Analysis results can be visualized to show structural deformations, stress distributions, strain patterns, and displacement profiles (Abedini & Zhang, 2021).

To carry out the simulation, a contact analysis is performed using LS+DYNA software the following five main steps: Select if the contact analysis is in LS-DYNA parametric design Language (APDL) or Workbench in this paper carries simulation done in LS-DYNA Workbench

- Create the model geometry and mesh.
- Identify the contact surfaces and materials for each part of the model.
- Define the solution options.
- Apply boundary conditions, normal force, and rotational speed for the disk pin in the simulation.
- Solve the contact problem.

Geometric Modeling

Two solid models are to be created in this module, which are pin and disc.

The assembled model of the pin and disc setup will as follow:

Dimension of Pin

Diameter: 6 mm

Height: 12 mm

When setting up a simulation the boundary conditions are crucial for ensuring accurate and meaningful results. Here are the typical boundary conditions considered:

Dimension of Disc

Diameter: 165 mm

Thickness: 10 mm

Loading condition

Load 20N and sliding speed 500rpm

The Disc is rigid and the pin is rotating

Contact Type: the board is kept rigid and the surface flexible to calculate the deformation of the pin itself. Friction contacts with very low COF and asymmetric behavior were chosen. Our findings the method is common for targeting on a per-node basis. We turned off the trim contact. These are all configuration parameters necessary for a rapid approach.

CHAPTER FOUR

RESULT AND DISCUSSION

4.1 Introduction

Experimental work was conducted to evaluate the effect of wear parameters (load, sliding speed, and track diameter) on the wear rate, specific wear rate, and coefficient of friction CFRPA material for horizontal, vertical and 45-degree orientation. To determine the ideal condition, 9 experiments for each orientation were conducted. Statistical analysis was then performed to determine the primary effects and choose the optimal settings based on the requirements. ANOVA was used to examine the response values obtained from wear test. For statistical studies, Minitab 21 software was used. Grey relational analysis was used for general (multiple) optimizations. the results obtained from the tensile test, hardness test, density and porosity test, and simulation results using LS-DYNA were discussed.

4.2 Hardness Test Result

Hardness refers to the resistance of a material to indentation, scratching, or other forms of deformation. Table 4-1 shows hardness test result from Vickers hardness test.

Table 4-1: Hardness test result

Samples	**Vickers hardness value (HV)**			
	Trial 1	Trial 2	Trial 3	Mean value
Horizontal orientation	86.3	82.2	76.5	81.6
45degree orientation	78.8	72.1	67.3	72.73
Vertical orientation	64.1	55.9	53.6	57.86

Figure 4-1 shows the Vickers hardness value of horizontal, vertical, and 45-degree orientation CFRPA6. The horizontal orientation exhibits the highest hardness value at approximately 82 HV. The 45-degree orientation follows, with a hardness value of around 75 HV, which, while slightly lower than the horizontal, still demonstrates significant hardness and robustness. The vertical orientation, however, shows the lowest hardness at about 60 HV. These variations in hardness values underscore the influence of print orientation on the mechanical properties of 3D orientation CFRPA6, with the horizontal orientation providing the highest hardness, making it preferable for applications requiring greater wear resistance Some works of the literature revealed the same results (Mudhaffer et al., 2024).

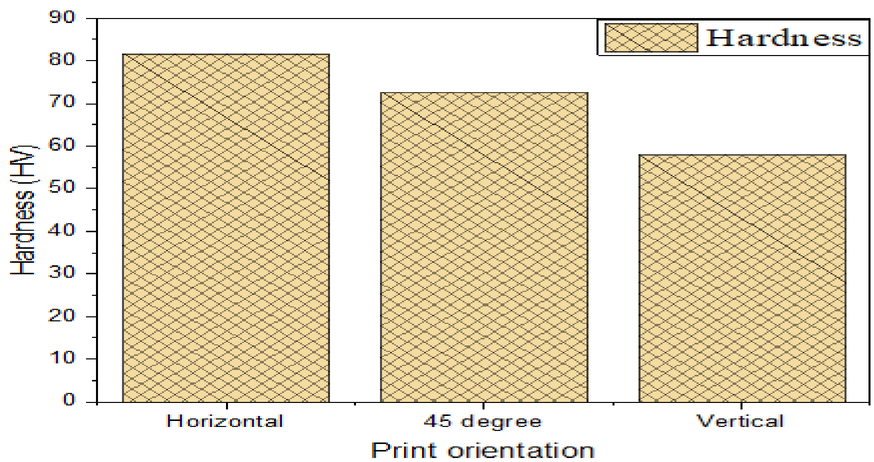

Figure 4-1: Bar plot for hardness test

4.3 Tensile Strength Test Result

The tensile strength of 3D orientation CFRPA6 varies significantly based on the orientation of the orientation layers. Figure 4-2 shows tensile strength result. The vertical orientation demonstrates the highest tensile strength, with a maximum stress of 0.0461MPa, indicating better load-bearing capacity and material performance under tension compared to other orientations. This superior tensile strength can be attributed to the optimized alignment of carbon fibers at this angle, providing enhanced reinforcement and load distribution. In contrast, the horizontal and 45degree orientations exhibit lower tensile strengths of 0.0194 MPa and 0.0203MPa, respectively, suggesting that the fiber alignment in these directions is less effective in resisting tensile forces. Similarly, the maximum strain for the vertical orientation reaches 0.2022, whereas the 45degree and horizontal orientations exhibit maximum strains of 0.0625 and 0.0898, respectively. The Figure 4-2 (b) shows fracture of sample after tensile test. These results indicate that the vertical orientation of 3D orientation CFRPA6 exhibits superior mechanical properties in terms of both stress and strain, highlighting its potential for applications requiring higher strength and flexibility.

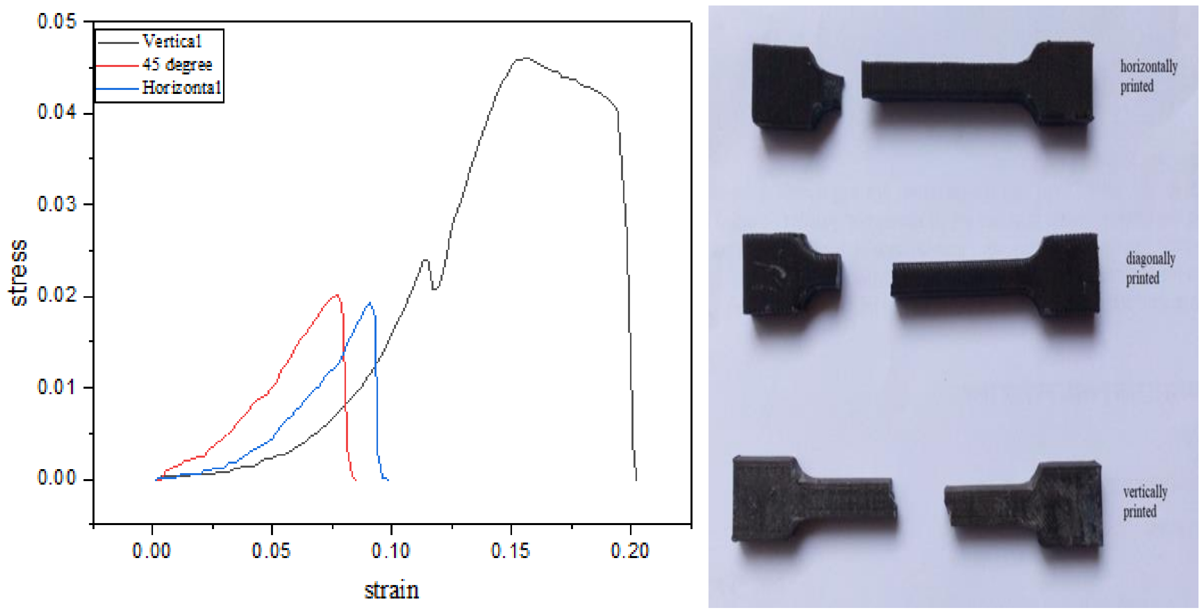

Figure 4-2: (a) Stress-strain diagram (b) Sample after tensile test

4.4 Analysis of Density and Porosity

The theoretical density for all samples is 1.232 g/cm³. The actual density measurements indicate that the horizontal orientation sample has the highest density at 1.219g/cm³, suggesting the best layer adhesion and least number of voids among the three orientations. The vertical orientation sample shows a slightly lower actual density of 1.211 g/cm³, reflecting minor increases in voids or layer gaps compared to the horizontal orientation. The 45-degree orientation sample has the lowest actual density at 1.215 g/cm³, indicating a higher presence of voids or less effective layer bonding. The horizontal orientation sample showing the lowest porosity at 1.03%, followed by the 45degree at 1.38%, and the vertical at 1.73%.

Table 4-2: Density and Porosity results

Sample	**Theoretical density (g/cm^3)**	**Actual density (g/cm^3)**	**Porosity %**
Horizontal orientation	1.232	1.219	1.03%
Vertical orientation	1.232	1.211	1.73%
45degree orientation	1.232	1.215	1.38%

4.5 Wear Optimization for Horizontal Orientation

Table 4-3 shows the calculated results of wear volume, wear rate, and specific wear rate using Eq. (3.8), (3.10), and (3.12) respectively. The weight of the sample before and after the wear test. The density of the material was 1.232g/cm^3.

Table 4-3 Analytical results for horizontal orientation

S. no	Load (N)	Speed (rpm)	Track diameter(mm)	Weight before test (g)	Weight after test (g)	Wear Volume (mm^3)	Wear rate (mm^3/m) *10^{-3}	Specific wear rate (mm^3/Nm) *10^{-4}	COF
1	10	200	30	0.3855	0.3844	0.91173	4.837	4.837	0.2023
2	**10**	**500**	**40**	**0.4134**	**0.4112**	**1.94346**	**2.32**	**2.32**	**0.2617**
3	10	800	50	0.3814	0.3781	2.91519	3.09	3.093	0.3195
4	20	200	40	0.3974	0.3953	1.85512	3.632	1.816	0.2711
5	20	500	50	0.4149	0.4117	2.82686	3.599	1.7	0.3365
6	20	800	30	0.3978	0.3947	2.73852	7.381	3.691	0.3489
7	30	200	50	0.3820	0.3789	2.99852	3.971	2.241	0.3583
8	30	500	30	0.3992	0.3955	3.16855	6.724	1.324	0.3271
9	30	800	40	0.4039	0.3996	3.99191	9.545	3.182	0.3875

4.5.1 Multi-response grey relational analysis for horizontal orientation

The signal-to-noise ratio data for wear rate, specific wear rate, and coefficient of friction were consolidated to determine the optimal parameter combination for minimizing wear and the coefficient of friction. An analysis was conducted on the wear parameters to achieve the lowest possible response. For improved performance, it is essential to reduce the wear at the surface of the pin. The values of S/N ratio, normalized S/N ratio, grey relational coefficient and grey relational grade for horizontal orientation listed in Table 4-4 and Table 4-5.

Step 1: Determine the S/N ratio for the respective responses using Eq (3.15), and (3.16).

Step 2: Normalization of the S/N values is the generation of grey relation within 0 and 1 using Equation 3.11.

Table 4-4: S/N ratio and Normalized S/N ratio values for horizontal orientation

S/N ratios			**Normalized Value**		
Wear rate	**Specific wear rate**	**COF**	**Wear rate**	**Specific wear rate**	**COF**
46.308	66.308	-13.880	0.652	0.000	1.000
52.690	72.690	-11.644	1.000	0.716	0.679
50.201	70.192	-9.911	0.893	0.496	0.367
48.797	74.818	-11.337	0.381	0.860	0.629
48.876	75.391	-9.460	0.823	0.893	0.275
42.638	68.657	-9.146	0.300	0.326	0.208
48.022	72.991	-8.915	0.771	0.739	0.158
43.447	77.562	-9.706	0.390	1.000	0.326
40.404	69.946	-8.235	0.000	0.471	0.000

Step 3: Calculation the grey relational coefficient using Eq. (3.19)

Step 4: The grey relational grade using Eq. (3.20)

Table 4-5: Grey relational co-efficient and grey relational grade values for horizontal orientation

Deviation Sequences			**Grey Relation Coefficient**			**GRG.**	**Rank**
Wear rate	**Specific wear rate**	**COF**	**Wear rate**	**Specific wear rate**	**COF**		
0.348	1.000	0.000	0.589	0.333	1.000	0.641	3
0.000	**0.284**	**0.321**	**1.000**	**0.638**	**0.609**	**0.749**	**1**
0.107	0.504	0.633	0.824	0.498	0.441	0.588	6
0.619	0.140	0.371	0.447	0.781	0.574	0.601	5
0.177	0.107	0.725	0.739	0.824	0.408	0.657	2
0.700	0.674	0.792	0.416	0.426	0.387	0.410	8
0.229	0.261	0.842	0.686	0.657	0.372	0.572	7
0.610	0.000	0.674	0.451	1.000	0.426	0.626	4
1.000	0.529	1.000	0.333	0.486	0.333	0.384	9

4.5.2 Analysis of mean for horizontal orientation GRG

The mean value of GRG for each factor i.e., wear rate, specific wear rate and COF at each level was also obtained using Minitab 21 for GRG and the result was listed in Table 4-6.

Table 4-6: Response table for a mean of GRG for horizontal orientation

Level	**Load (N)**	**Sliding speed(rpm)**	**Track diameter (mm)**
1	**0.6593**	0.6047	0.5590
2	0.5560	**0.6773**	0.5780
3	0.5273	0.4607	**0.6057**
Delta	0.1320	0.2167	0.0467
Rank	2	1	3

The factor with the greatest effect on the mean was the sliding speed (Delta = 0.6773, Rank = 1). The factor with the least effect on the mean was Track diameter (Delta = 0.6057, Rank = 3). To find out the predicted value of the responses (GRG the following linear regression equation was used as mentioned (Chavhan & Wankhade, 2021).

$$\text{Opt} = A1+B2+C3 -2m \quad (4.1)$$

Optimum = 0.6593+ 0.6773+ 0.6057-2 x 0.58089

Opt = 0.7805 (Predicted optimum value of GRG)

Where m is the average performance mean value for GRG (i.e.: m=0.58089).

Figure 4-3, showed that the main effects plot for the means of three different variables: load, sliding speed, and track diameter. The maximum point for load at level 3, speed at level 3, and TD at level 2. This justified the optimum parameter was at the lowest load, lowest track diameter, and lower speed as (**A1B2C3)**. As the load increases from 10 to 30, the mean value of the response variable decreases, indicating that increasing the load has a negative effect on the response. The mean value increases sharply as the sliding speed increases from 200 to 500, suggesting that higher sliding speeds have a positive effect on the response. However, the mean value then decreases as the sliding speed goes beyond 500. The mean value increases steadily as the track diameter increases from 30 to 50, implying that larger track diameters have a positive impact on the response.

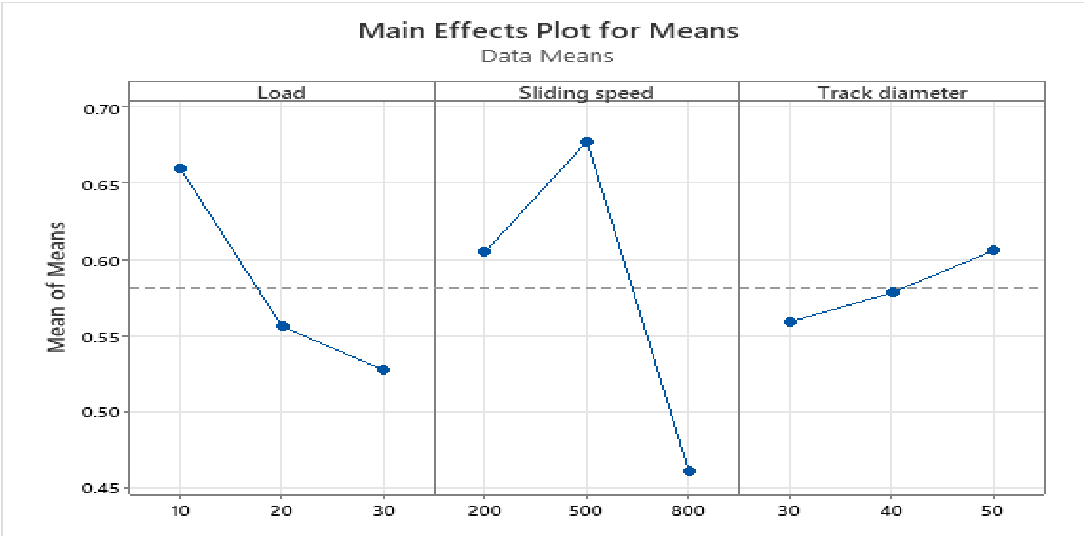

Figure 4-3: Interaction effect of mean plot

4.5.3 Analysis of S/N ratio for horizontal orientation GRG

The analysis involves a detailed examination of various parameters and their impact on performance. By investigating the main effects and interactions of factors such as load, sliding speed, and track diameter, insights are gained into optimizing the S/N ratio for horizontal printing. Table 4-5 shows the S/N ratio for GRG. Sliding speed has the most significant effect on the signal-to-noise ratio with value of -3.409, load has the second most important impact on the SN ratio with the value of -3.662. Track diameter has the smallest effect on the SN ratio compared to the other two factors.

Table 4-7: Signal to Noise ratios for GRG (larger is better) for horizontal orientation

Level	**Load**	**Sliding speed**	**Track diameter**
1	**-3.662**	-4.379	-5.225
2	-5.272	**-3.409**	-5.082
3	-5.745	-6.890	**-4.371**
Delta	2.083	3.481	0.854
Rank	2	1	3

Figure 4-4, shows the control factor's main effect plot for the S/N ratio and the optimal parameter combination on GRG response (larger the better GRG response). In the S/N ratio, the numerical value of the maximum point in each graph shows the best optimum combination of factors at that level and the above figure shows the maximum point for Load at level 3 of 30N, for Sliding speed level 3 of 800RPM and Track diameter of level 2 of 40mm that is (**A1B2C3**) was selected. The most effective parameter of GRG response is the sliding speed when compared with other factors and Track diameter that have the least effect on the GRG response.

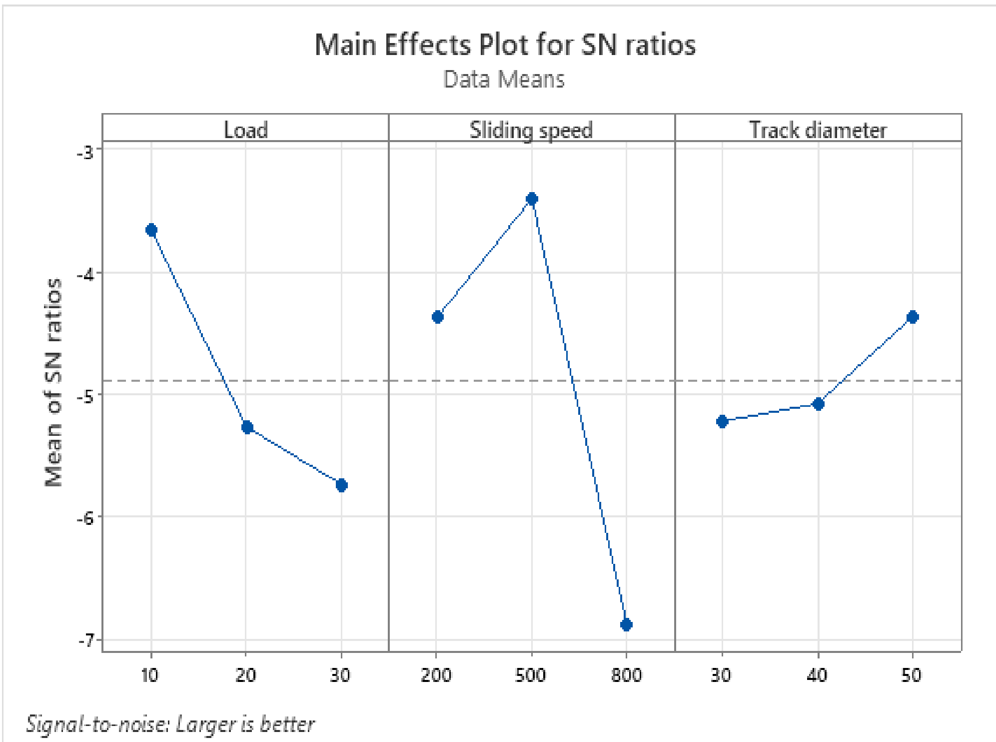

Figure 4-4: main effect plot for S/N ratio horizontal orientation

4.5.4 Determining optimum condition for horizontal orientation GRG

The optimum prediction condition for the S/N ratio in which, the GRG response result of the material was obtained with the terms set was shown in Table 4-8. The selected optimum parameters in this study were **A1B2C3**.

Table 4-8: prediction values for horizontal orientation

Factors	Levels	Value of level	Rank of affecting	Prediction Values	
				S/N Ratio	Mean
Load	3	30N	1	-1.65656	0.7514
Sliding speed	3	800 RPM	2		
Track diameter	1	40 mm	3		

4.5.5 Analysis of variance for horizontal orientation GRG

ANOVA was employed as an analytical tool to identify the significant factors in the measurements by examining the relationship between the response variable and the proposed factors(Gajalakshmi et al., 2019).

Regression equation

$$\mathrm{GRG} = 0.740 - 0.0066\mathrm{L} - 00024\ SS + 0.00237\ \mathrm{TD} \qquad (4.2)$$

Table 4-9 shows that sliding speed is the dominant factor influencing the grey relation grade, contributing 67.42% to the total variation. Load is also a significant factor, contributing 26.78% and track diameter is statistically significant, contributing only 3.05%.

Table 4-9: ANOVA analysis for horizontal orientation

Source	DF	Adj SS	Adj MS	F-Value	P-Value	%Contribution
Load	2	0.028924	0.014462	9.59	0.094	26.78
Sliding speed	2	0.072961	0.036480	24.19	0.040	67.42
Track diameter	2	0.003304	0.001652	1.10	0.477	3.05
Error	2	0.003016	0.001508			3.01
Total	8	0.108205				

The normal probability plot shown in Figure 4-5 was used to assess whether the residuals of the response variable (Grade) follow a normal distribution. The x-axis represents the residuals, ranging from approximately -0.10 to 0.15, and the y-axis represents the cumulative percentage from 1% to 99%. The plot shows blue dots representing the observed residuals plotted against a red diagonal line, which represents the expected normal distribution.

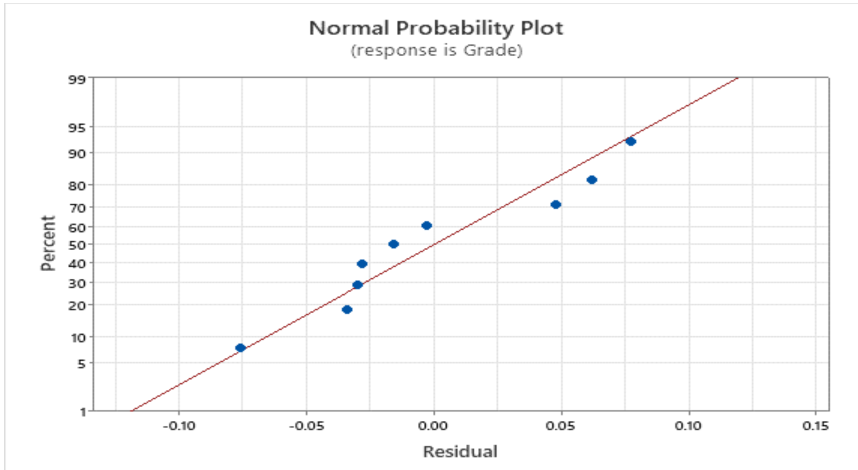

Figure 4-5: Normal probability plot for grade for horizontal orientation

Figure 4-4 (a) illustrates the relationship between GRG, load, and sliding speed in a wear optimization study. The values are represented by the different color regions and contour lines. As the Sliding speed increases and the Load decreases, the GRG values generally improve, indicating a more favorable response. Figure 4-6 (b) shows the relationship between GRG, load, and track diameter and the GRG values are higher in the region where the track diameter is around 40-50 and the load is around 10-20. This suggests that this combination of factors results in the optimal or desired response. As the load increases and the track diameter decreases, the GRG values tend to decrease, indicating a less favorable response.

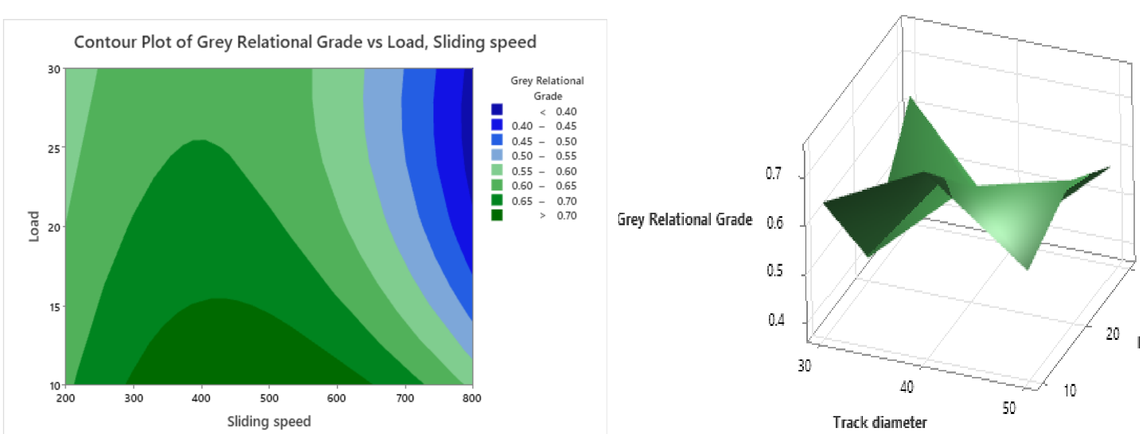

Figure 4-6: (a) contour plot for horizontally oriented GRG and (b) 3D Surface plot

4.6 Wear Optimization for Vertical Print Orientation

Wear optimization for vertical print orientation involves a comprehensive analysis that integrates wear test results, signal-to-noise (S/N) ratio analysis, nominal values, grey relational coefficients, and grey relational grades. This approach aims to identify the most suitable printing parameters and material compositions that minimize wear and enhance durability in vertical orientations. Table 4-10 shows the analytical result of wear volume, wear rate and specific wear rate using Eq. (3.8), (3.10) and (3.12) respectively. Also, the weight of the sample before and after the wear test is measured using weight balance.

Table 4-10: Analyzed result for Vertical orientation

S no:	Load (N)	Speed (rpm)	Track diameter(mm)	Weight before test (g)	Weight after test (g)	Wear Volume(mm^3)	Wear rate(mm^3/m)*10^{-3}	Specific wear rate (mm^3/Nm)*10^{-4}	COF
1	10	200	30	0.3977	0.3944	1.577	3.832	3.824	0.345
2	**10**	**500**	**40**	**0.4066**	**0.4029**	**2.402**	**3.226**	**3.226**	**0.35**
3	10	800	50	0.3865	0.3824	4.054	6.013	6.013	0.428
4	20	200	40	0.3891	0.3842	2.628	4.015	2.01	0.362
5	20	500	50	0.4149	0.4096	3.153	4.48	2.24	0.403
6	20	800	30	0.3948	0.389	3.378	9.045	4.23	0.433
7	30	200	50	0.3793	0.3727	3.829	8.603	2.87	0.471
8	30	500	30	0.3917	0.3848	4.054	4.331	1.44	0.469
9	30	800	40	0.3859	0.3786	4.354	1.2188	4.06	0.475

4.6.1 Multi-response grey relational analysis for vertical orientation

Vertical print orientation also follows the same steps as horizontal print orientation. S/N ratio, normalized value, grey relational coefficient and grey relational grade values for vertical orientation listed in Table 4-11 and Table 4-12.

Step 1: Determine the S/N ratio for the respective responses using Eq. (3.15), and (3.16).

Step 2: Normalization of the S/N values is the generation of grey relations within 0 and 1 using Eq. (3.17).

Table 4-11: S/N ratio and normalized value for vertical orientation

S/N ratios			**Normalized Value**		
Wear rate	**Specific wear rate**	**COF**	**Wear rate**	**Specific wear rate**	**COF**
48.331	68.350	-9.244	0.932	0.479	1.000
49.827	69.827	-9.119	1.000	0.609	0.962
44.418	64.418	-7.371	0.689	0.000	0.362
47.926	73.936	-8.826	0.329	0.875	0.869
46.974	72.995	-7.894	0.860	0.825	0.554
40.872	67.473	-7.270	0.351	0.390	0.323
41.307	70.842	-6.540	0.400	0.687	0.031
47.268	76.833	-6.577	0.877	1.000	0.046
38.281	67.829	-6.466	0.000	0.427	0.000

Step 3: Calculate the grey relational coefficient using Eq. (3.19).

Step 4: The grey relational grade using Eq. (3.20)

Table 4-12: Grey relational co-efficient and GRG values for vertical orientation

Deviation Sequences			**Grey Relation Coefficient**			**GRG.**	**Rank**
Wear volume	**Specific wear rate**	**COF**	**Wear volume**	**Specific wear rate**	**COF**		
0.068	0.521	0.000	0.881	0.490	1.000	0.790	2
0.000	**0.391**	**0.038**	**1.000**	**0.561**	**0.929**	**0.830**	**1**
0.311	1.000	0.638	0.617	0.333	0.439	0.463	7
0.671	0.125	0.131	0.427	0.800	0.793	0.673	5
0.140	0.175	0.446	0.781	0.741	0.528	0.684	4
0.649	0.610	0.677	0.435	0.450	0.425	0.437	8
0.600	0.313	0.969	0.455	0.615	0.340	0.470	6
0.123	0.000	0.954	0.802	1.000	0.344	0.715	3
1.000	0.573	1.000	0.333	0.466	0.333	0.378	9

4.6.2 Analysis of mean for vertical orientation GRG

Analyzing the mean values for vertical orientation and their associated GRG involves a detailed examination of key parameters and their effects on performance. By evaluating factors such as load, sliding speed, and track diameter, insights are gained into optimizing the mean values for vertical printing. The mean value of GRG for each factor i.e., wear rate, specific wear rate and COF at each level was also obtained using Minitab 21 for GRG and the result was listed in Table 4-13.

Table 4-13: Response table of means for vertical orientation

Level	**Load**	**Sliding speed**	**Track diameter**
1	**0.6943**	0.6443	**0.6473**
2	0.5980	**0.7430**	0.6270
3	0.5210	0.4260	0.5390
Delta	0.1733	0.3170	0.1083
Rank	2	1	3

The factor with the greatest effect on the mean from above Table 4-13 was the sliding speed of (Delta = 0.7430, Rank = 1). Track diameter was the factor with the least effect on the mean (Delta = 0.6473, Rank = 3). To find out the predicted value of the responses (GRG the following linear regression equation was used as mentioned

$$\text{Optimum value} = A1+B2+C1-2m \quad (4.3)$$

Optimum value = 0.6943 + 0.7430 + 0.6473- 2 x 0.604433

Opt = 0.8757 (Predicted optimum value of GRG)

Figure 4-7 shows main effect plot for means. The main effects plot for means indicates that as Load increases from 10 to 30, the response variable decreases from approximately 0.70 to 0.50. For Sliding Speed, the response first increases from around 0.65 at 200 to 0.75 at 500, then decreases to about 0.45 at 800. Similarly, as Track Diameter increases from 30 to 50, the response decreases from roughly 0.60 to 0.45. Overall, increasing Load and Track Diameter consistently reduce the response, while Sliding Speed shows a non-linear effect, increasing the response up to a point before decreasing.

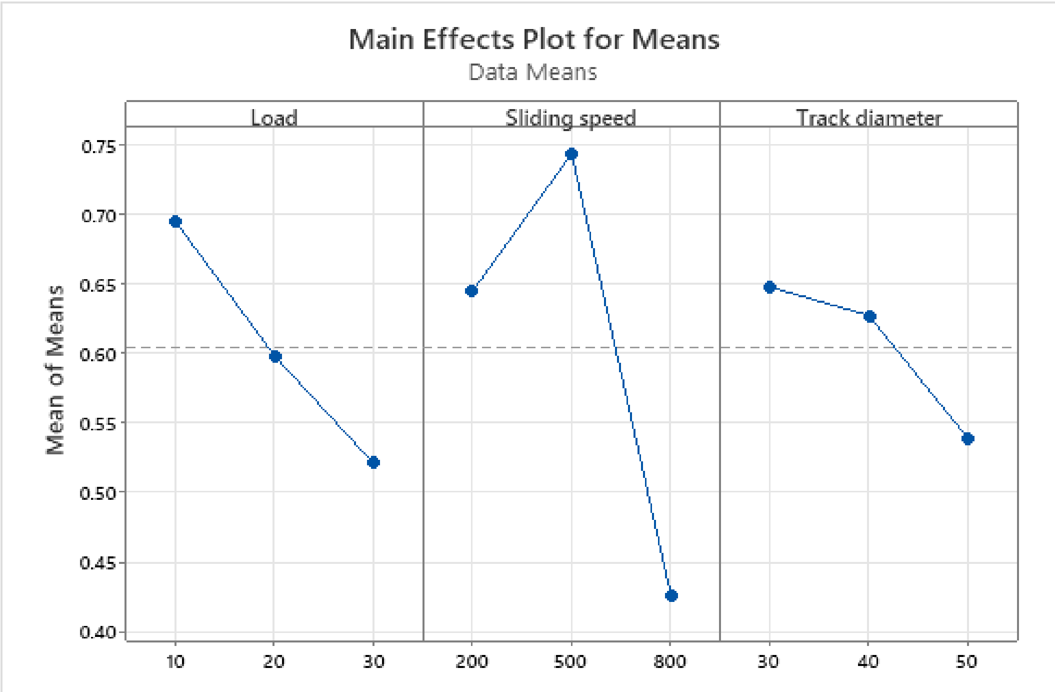

Figure 4-7: Main effect plots for means of vertical orientation

4.6.3 Analysis of S/N ratio for vertical orientation GRG

The S/N ratio of GRG for each factor i.e., wear rate, specific wear rate and COF at each level was also obtained using Minitab 21 for GRG and the result was listed in Table 4-14.

Table 4-14: Response table for signal to noise Ratio (Larger is better) for vertical orientation

Level	**Load**	**Sliding speed**	**Track diameter**
1	-3.451	-4.015	-4.051
2	-4.643	-2.610	-4.503
3	-5.974	-7.443	-5.515
Delta	2.523	4.833	1.465
Rank	2	1	3

Figure 4-8 shows main effect plot for vertical printed SN ratio. The main effects plot for SN ratios indicates that increasing Load and Track Diameter both decrease the SN ratio, leading to poorer performance. For Sliding Speed, the SN ratio initially increases, indicating better performance up to a certain point, before it decreases again, suggesting an optimal speed range.

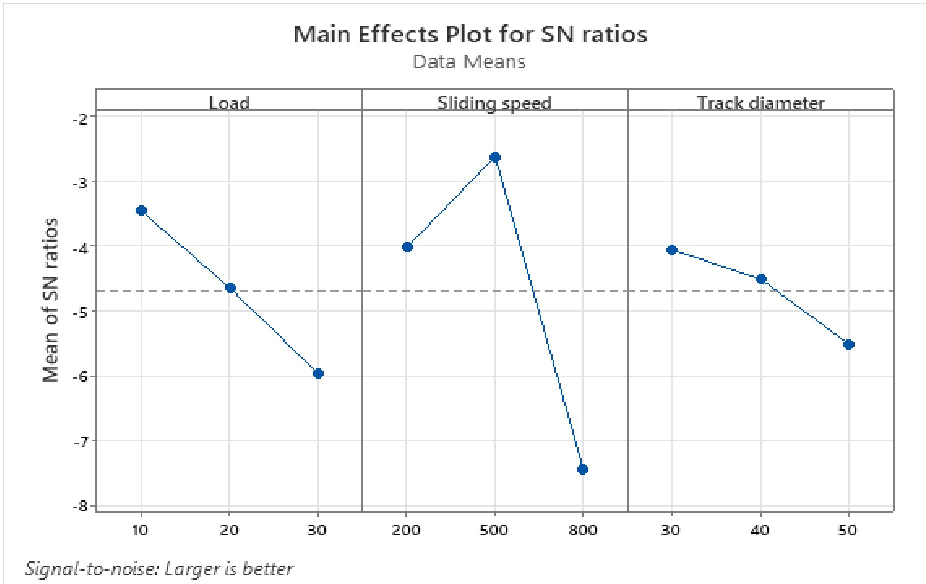

Figure 4-8: Main effects plot for SN ratios vertical orientation

4.6.4 Determining optimum condition for vertical orientation GRG

The optimum prediction condition for the S/N ratio in which, the GRG response result of the material was obtained with the terms set was shown in Table 4-15. The selected optimum parameters in this study were lowest load, lower sliding speed and a lowest track diameter which was **A1B2C1**.

Table 4-15: prediction values for vertical orientation

Factors	**Levels**	**Value of level**	**Rank of affecting**	**Prediction Values S/N Ratio**	**Mean**
Load	1	10*N*	2	-0.7334	0.8365
Sliding speed	2	500 RPM	1		
Track diameter	1	30 mm	3		

4.6.5 Analysis of variance for GRG vertical orientation

The ANOVA of the GRG for vertically printed parts can reveal the relative significance of process parameters on the composite's tribological performance and wear characteristics. Table 4-16 shows that sliding speed is the dominant factor influencing the grey relation grade, contributing 69.88 to the total variation. Load is also a significant factor, contributing 20% and track diameter is statistically significant, contributing only 8.68%.

Regression equation

$$GRG = 1.176 - 0.00876L – 0.000364SS - 0.00542TD \quad (4.4)$$

Table 4-16: ANOVA analysis for vertical orientation

Source	**DF**	**Adj SS**	**Adj MS**	**F-Value**	**P-Value**	**Contribution %**
Load	2	0.045254	0.022627	15.53	0.060	20
Sliding speed	2	0.157894	0.078947	54.19	0.018	69.88
Track diameter	2	0.019894	0.009947	6.83	0.128	8.68
Error	2	0.002914	0.001457			1.29
Total	8	0.225954				

In Figure 4-9 the normal probability plot shows the relationship between the residuals (differences between observed and expected Grey Relational Grade values) and the corresponding probabilities. The close alignment of the data points (blue circles) along the red line indicates that the residuals follow a normal distribution, which is an important assumption for many statistical analyses. The tight clustering of the data points around the straight line suggests the Grey Relational Grade values are normally distributed, providing confidence in the validity of the underlying data and analyses.

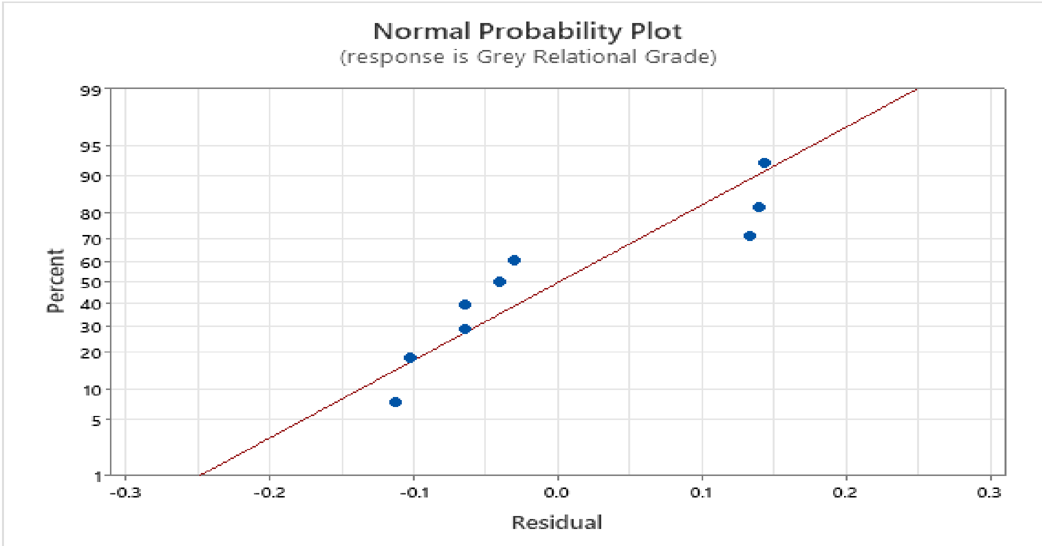

Figure 4-9: Normal probability plot for grade for vertical orientation

Figure 4-10 (a) illustrates contour plot of GRG versus load and sliding speed. Higher GRG are represented by darker shades of green. Lower and higher extremes of both load and sliding speed result in lower GRG, indicating poorer performance. This suggests that there is a specific range of load and sliding speed that maximizes the GRG. Figure 4-10 (b) shows the relationship between load, track diameter, and GRG. The plot indicates that the optimal region, with the highest GRG values, is where the track diameter is around 40-50 and the load is around 10-20. As the load increases and the track diameter decreases, the GRG values tend to decline, suggesting less favorable system performance.

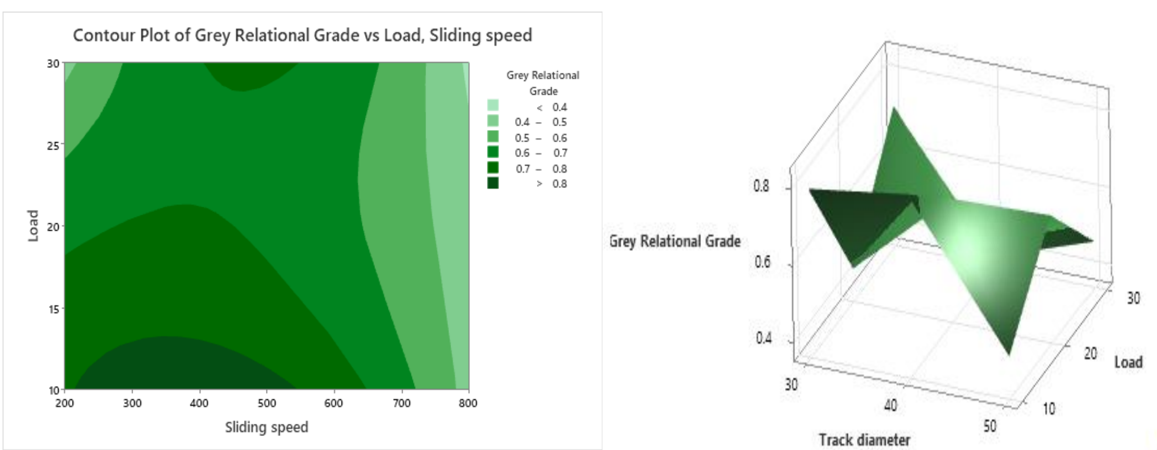

Figure 4-10: (a) contour plot for vertically printed GRG and (b) 3D Surface plot

4.7 Wear Optimization of 45degree Orientation

Table 4-17 shows the calculated results of wear volume, wear rate, and specific wear rate using Eq. (3.8), (3.10), and (3.12) respectively. The weight of the sample before and after the wear test.

Table 4-17: Analyzed result for 45degree orientation

S. no	**Load (N)**	**Speed (rpm)**	**Track diameter (mm)**	**Weight before test (g)**	**Weight after test (g)**	**Wear Volume (mm^3)**	**Wear rate(mm^3/m)*10^{-3}**	**Specific wear rate(mm^3/Nm)*10^{-4}**	**COF**
1	10	200	30	0.3965	0.3943	1.2987	3.488	3.488	0.282
2	**10**	**500**	**40**	**0.4193**	**0.4165**	**2.1915**	**2.454**	**2.454**	**0.288**
3	10	800	50	0.4185	0.4152	3.0844	5.89	5.89	0.313
4	20	200	40	0.3671	0.3632	2.2727	3.768	1.86	0.343
5	20	500	50	0.4143	0.4101	2.9221	5.721	1.88	0.369
6	20	800	30	0.3628	0.3580	2.8409	9.043	4.52	0.371
7	30	200	50	0.4157	0.4104	3.4091	7.751	2.58	0.411
8	30	500	30	0.3780	0.3723	3.6526	3.956	1.32	0.409
9	30	800	40	0.3938	0.3874	3.9773	10.851	3.62	0.415

4.7.1 Multi-response grey relational analysis for 45degree orientation

45-degree print orientation also follows the same steps as horizontal print orientation.

Step 1: Determine the S/N ratio for the respective responses using Eq. (3.15), and (3.16).

Step 2: Normalization of the S/N values is the generation of grey relations within 0 and 1 using Eq. (3.17) and Eq. (3.18)

Table 4-18: S/N ratio and normalized value for 45degree orientation

S/N ratios			Normalized Value		
Wear volume	**Specific wear rate**	**COF**	**Wear volume**	**Specific wear rate**	**COF**
43.236	63.236	-10.995	0.472	0.000	0.000
49.148	69.143	-10.812	0.877	0.610	0.045
52.199	72.217	-10.089	1.000	0.797	0.233
40.874	66.897	-9.294	0.833	0.425	0.459
48.589	74.510	-8.659	0.849	0.903	0.654
48.478	74.517	-8.613	0.844	0.899	0.669
39.291	68.826	-7.766	0.000	0.587	0.955
42.213	71.768	-7.723	0.369	0.774	0.970
48.008	77.589	-7.639	0.819	1.000	1.000

Step 3: Calculation the grey relational coefficient using Eq. (3.19)

Step 4: The grey relational grade using Eq. (3.20)

Table 4-19: Grey relational co-efficient and grey relational grade values for 45degree orientation

Deviation Sequences			Grey Relation Coefficient			GRG.	Rank
Wear volume	**Specific wear rate**	**COF**	**Wear volume**	**Specific wear rate**	**COF**		
0.528	1.000	1.000	0.486	0.333	0.333	0.384	9
0.123	0.390	0.955	0.803	0.562	0.344	0.569	7
0.000	0.203	0.767	1.000	0.711	0.395	0.702	4
0.167	0.575	0.541	0.750	0.465	0.480	0.565	8
0.151	0.097	0.346	0.768	0.838	0.591	0.732	2
0.156	0.101	0.331	0.762	0.833	0.602	0.732	3
1.000	0.413	0.045	0.333	0.548	0.917	0.599	6
0.631	0.226	0.030	0.442	0.689	0.943	0.691	5
0.181	0.000	0.000	0.734	1.000	1.000	0.911	1

4.7.2 Analysis of mean for 45degree orientation GRG

The mean value of GRG for each factor i.e., wear volume, specific wear rate and coefficient of wear rate at each level was also obtained using Minitab 21 for GRG and the result was listed below.

Table 4-20: Response table of means for 45degree orientation

Level	**Load**	**Sliding speed**	**Track diameter**
1	**0.7187**	0.6120	**0.6253**
2	0.5330	**0.7183**	0.6127
3	0.5190	0.4403	0.5327
Delta	0.1997	0.2780	0.0927
Rank	2	1	3

The factor with the greatest effect on the mean from the above Table 4-20 was the sliding speed of (Delta = 0.7183, Rank = 1). Track diameter was the factor with the least effect on the mean (Delta = 0.6253, Rank = 3). To find out the predicted value of the responses (GRG the following linear regression equation was used as mentioned

$$Opt = A1+B2+C1 -2m \quad (4.5)$$

Optimum = 0.7187+ 0.7183+ 0.6253-2 x 0.5902

Opt = 0.8819 (Predicted optimum value of GRG, where m is average value, m=0.5902)

Figure 4-11: Main effect plot for means of 45degree orientation

4.7.3 Analysis of S/N ratio GRG for 45degree orientation

The analysis focuses on the impact of various parameters on performance. By examining the main effects plot, one can identify how factors such as load, sliding speed, and track diameter influence the mean S/N ratios. Table 4-21 shows response table for signal to noise ratio.

Table 4-21: Response table for signal to noise Ratio (Larger is better) for 45degree orientation

Level	**Load**	**Sliding speed**	**Track diameter**
1	-3.061	-4.436	-4.385
2	-5.591	-2.971	-4.709
3	-5.952	-7.198	-5.510
Delta	2.891	4.227	1.125
Rank	2	1	3

Figure 4-12 shows a main effects plot for the SN ratios in a 45-degree orientation. The plot illustrates the relationships between load, sliding speed, and track diameter and their impacts on the mean SN ratios.

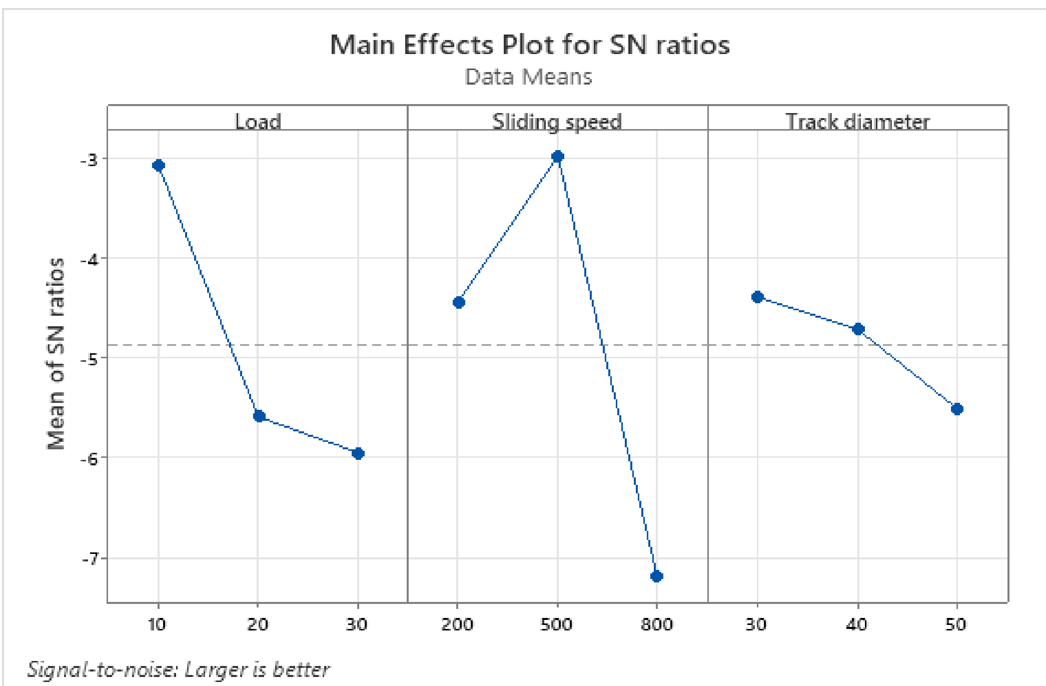

Figure 4-12: Main effect plots for SN ratios 45degree orientation

4.7.4 Determining optimum condition GRG for 45degree orientation

The optimum prediction condition for the S/N ratio in which, the GRG response result of the material was obtained with the terms set was shown in Table 4-22. The selected optimum parameters in this study **A1B2C1.**

Table 4-22: prediction values for 45degree orientation

Factors	Levels	Value of level	Rank of affecting	Prediction Values S/N Ratio	Prediction Values Mean
Load	1	10*N*	2	- 0.881889	0.681194
Sliding speed	2	200 RPM	1		
Track diameter	1	30 mm	3		

4.7.5 Analysis of variance GRG for 45degree orientation

ANOVA was employed as an analytical tool to identify significant factors in the measurements by examining the relationship between the response variable and the proposed factors. Table 4-23 shows that sliding speed is the dominant factor influencing the grey relation grade, contributing 56.68% to the total variation. Load is also a significant factor, contributing 35.78% and track diameter is statistically significant, contributing only 7.27%.

Regression equation

$$\text{GRG} = 0.118 - 0.00998 - 0.000286 - 0.00463\ \text{TD} \quad (4.6)$$

Table 4-23: ANOVA analysis for 45degree orientation

Source	DF	Adj SS	Adj MS	F-Value	P-Value	Contribution %
Load	2	0.074535	0.037267	137.29	0.007	35.78
Sliding speed	2	0.118060	0.059030	217.47	0.005	56.68
Track diameter	2	0.015148	0.007574	27.90	0.035	7.27
Error	2	0.000543	0.000271			1.92
Total	8	0.208286				

Figure 4-13 shows the normal probability plot for the residuals, with the response being Grade, which is used to assess the normality of the residuals. The horizontal axis represents the residuals (differences between observed and predicted values), while the vertical axis shows the cumulative probability. Ideally, the points should align closely with the red diagonal line if the residuals are normally distributed. In this plot, the points follow the line, indicating that the residuals are approximately normally distributed, with only slight deviations at the extremes. This suggests that the assumption of normality for the residuals is reasonably satisfied.

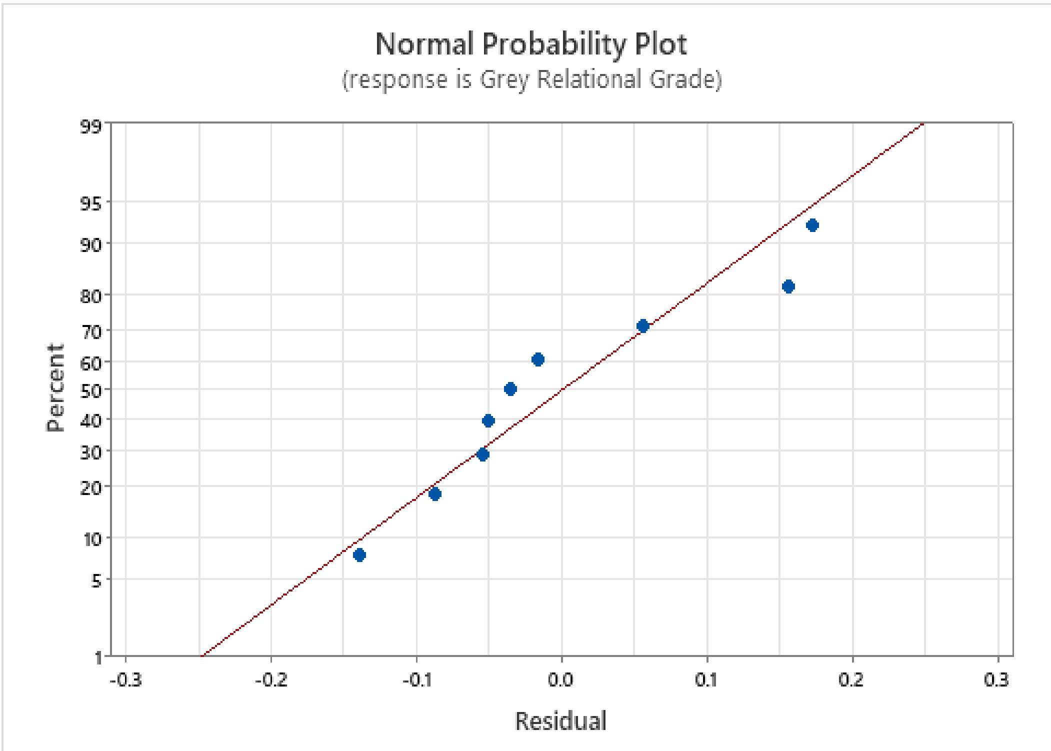

Figure 4-13: Normal probability plot for grade for 45degree orientation

In Figure 4-14 (a) the contour plot shows the relationship between GRG, load, and track diameter. The color-coded contour lines represent different GRG value ranges, with the higher values (closer to 0.8) indicating more desirable system performance. The plot reveals that the optimal region, where the GRG is maximized, occurs at a Track diameter around 40-45 and a Load around 10-15. In Figure 4-14 (b) the 3D surface plot visualizes the relationship between (GRG), Load, and Sliding speed. The green surface represents the GRG values, with higher values indicating more desirable system performance. The plot shows that the optimal region, where the GRG is maximized, occurs at a Sliding speed around 500-600 and a Load around 10-15.

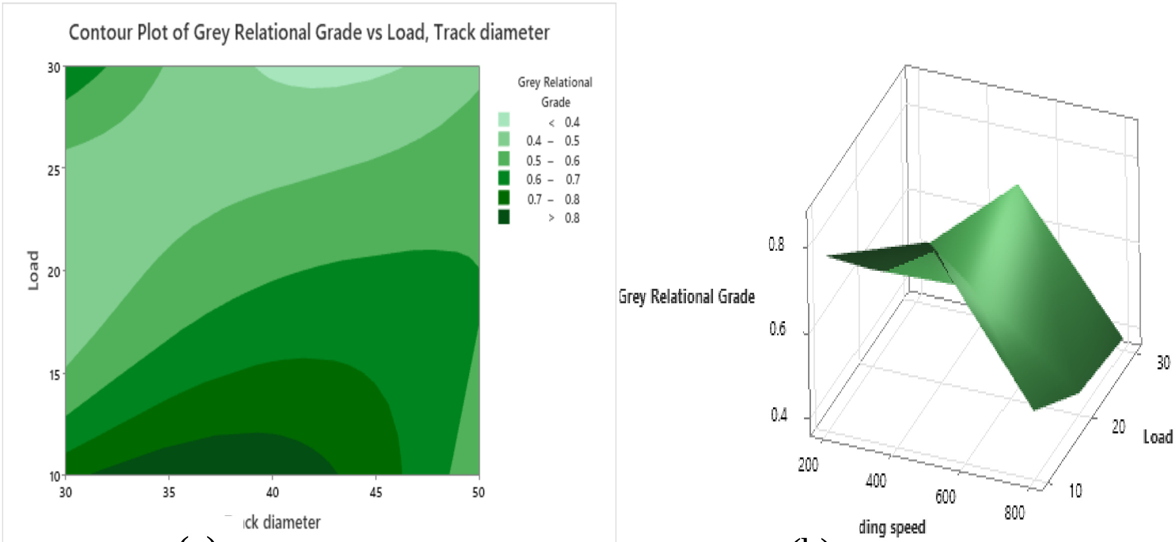

(a) (b)

Figure 4-14: (a) contour plot for 45degree orientation and (b) 3D Surface plot

4. 8 Confirmation Test

In the experimental design, the confirmation test is the final step to verify the values predicted using the optimal levels in Minitab-21 for the frictional coefficient and wear rate. To determine if the values obtained from the experiment and GRA are accurate, they are evaluated and presented in Tables 4-24. The percentage of error were less than 5% so the proposed result was validated with experimental results.

$$Error = \frac{(Experimented\ value - predicated\ value}{Experimented\ value} \times 100 \tag{4.7}$$

Table 4-24: Confirmation location from Grey Relational Grade (GRG) for all 3DOrientation value

S. No	Response	Optimum value	Predicted value	Experimented value	Error %
1	Horizontal Orientation	10, 500,50	0.7514	0.7805	3.73
2	Vertical Orientation	10, 500,30	0.8365	0.8758	4.48
3	45 degree	10, 500,30	0.681194	0.8819	2.27

4.9 Scanning Electron Microscope Examination

SEM is a powerful analytical tool used to observe and analyze the surface morphology and microstructural features of materials at high magnifications. It is a type of electron microscope that takes photographs of a material by scanning its surface with a concentrated beam of electrons. The electrons interact with atoms in the sample, producing distinct signals that carry information on the surface topography and composition of the sample.

4.9.1 SEM analysis of worn surface

SEM was used to investigate the worn surface of carbon fiber-reinforced polymer composites in chosen samples. Figure 4-15 shows the surface morphology and microstructural features of the composite after wear test. The images were captured at magnification of 600x and 1000x, with scale of 20µm and 50µm. The irregular, uneven surface texture suggests significant material removal and damage during the wear process. Distinct wear tracks are visible, running parallel to the direction of sliding motion. These tracks suggest the primary direction of wear and highlight the regions where the material has been most affected by the sliding action.

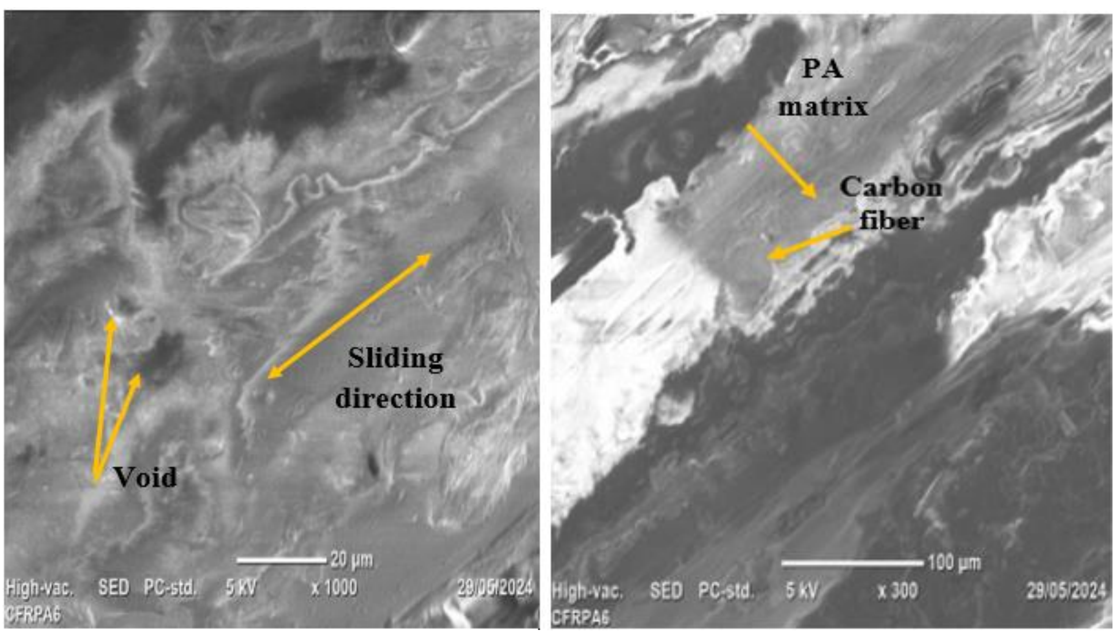

Figure 4-15: SEM image of worn surface for horizontal orientation sample 2

4.9.2 SEM analysis of fracture surface after tensile test

The failure mechanisms and the integrity of the fiber-matrix interface, a detailed analysis of the fracture surfaces using SEM is essential. Figure 4-16 shows the fracture surface of the composite after tensile test. The micrography provides a detailed view of the microstructural features at magnification of 100x and 600x. Some fibers were pulled out from the matrix, indicating the fiber-matrix adhesion strength. This suggests the effectiveness of load transfer between the fibers and the polymer matrix and some fibers were broken rather than pulled out, suggesting that the fibers reached their tensile limit before the matrix. The rough texture suggests that both the matrix and the fibers contributed to the fracture process.

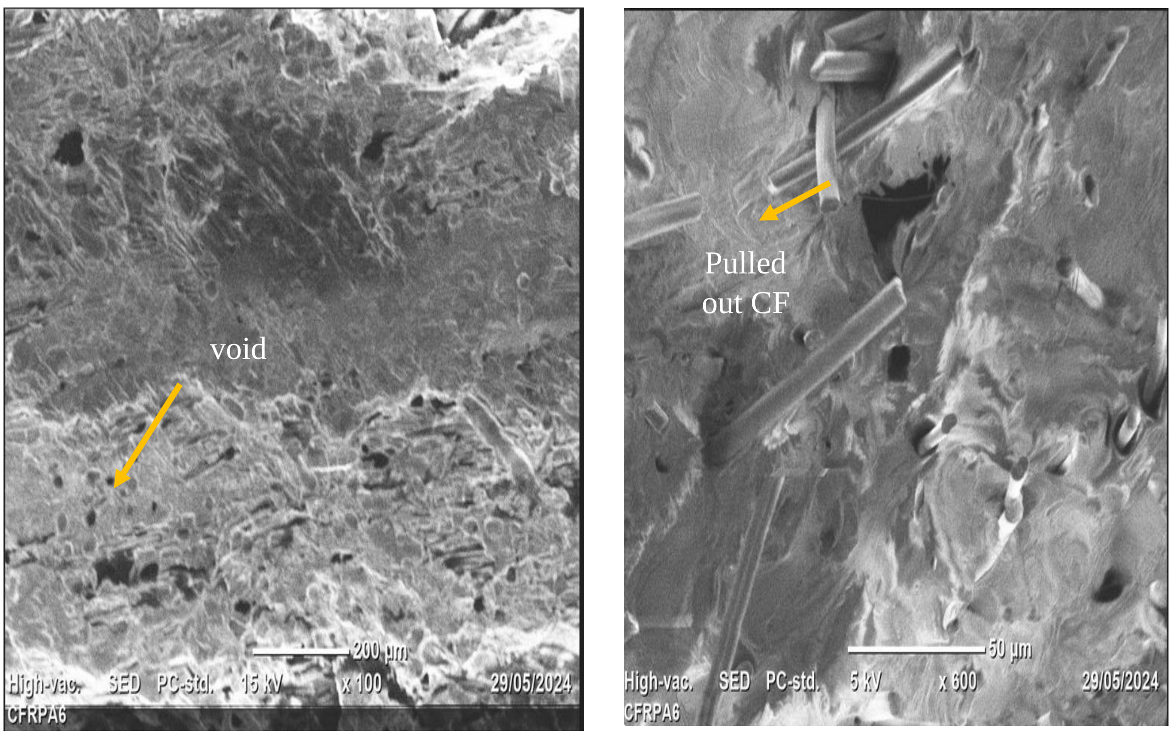

Figure 4-16: SEM analysis of fracture surface after tensile test for vertical orientation

4.10 Simulation result obtained from LS DYNA

The analysis of equivalent stress and total deformation was conducted using LS-DYNA software for horizontally, vertically and diagonally orientation CFRPA. The simulation was conducted at a sliding speed of 500rpm and load of 20N. The mesh was discretized by 15 as shown in Figure 4-17. The comparative assessment was done for print orientations.

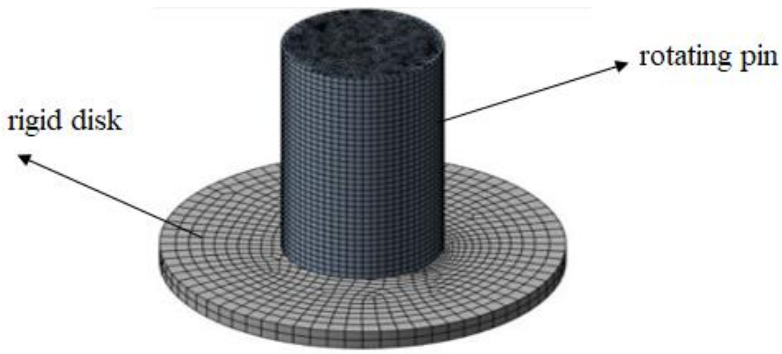

Figure 4-17: Mesh analysis of CFPA by LS DYNA

4.10.1 Equivalent stress result

In LS-DYNA simulations the equivalent stress is a critical parameter for evaluating the material's response to applied loads. The equivalent stress is calculated from the stress components within the material and is used to predict yielding under complex loading conditions. The value of equivalent stress can vary significantly based on the print orientation due to the anisotropic nature of 3D printed composites. Figure 4-18 (a) shows the stress distribution in horizontal print orientation. The small red region shows the maximum equivalent stress of 1.491 MPa, whereas the light blue color indicates the points where the equivalent stress is a minimum of 0.02395 MPa. The stress distribution is focused in the center of the structure, indicating that the horizontal orientation induces the highest stresses in this area. Figure 4-18 (b) shows the stress distribution in a 45-degree print orientation. The maximum equivalent stress is 2.146MPa, which is higher than the vertical orientation. Whereas, the minimum equivalent stress was 0.01464MPa. The stress distribution is more evenly spread across the structure, with the highest stresses still concentrated in the central region. Figure 4-18 (c) shows the stress distribution in vertical print orientation. The red region shows the maximum equivalent stress of 4.117MPa, which is significantly higher than the other two print orientation cases. Whereas, the dark blue color indicates the points where the equivalent stress is a minimum 0.02585MPa. Comparing the maximum equivalent stress values, the horizontal orientation has the lowest stress of 1.491MPa, followed by the 45-degree orientation at 2.146MPa, and the vertical orientation has the highest stress of 4.117MPa. Figure 4-19 shows the graphical representation of equivalent stress for the print orientations.

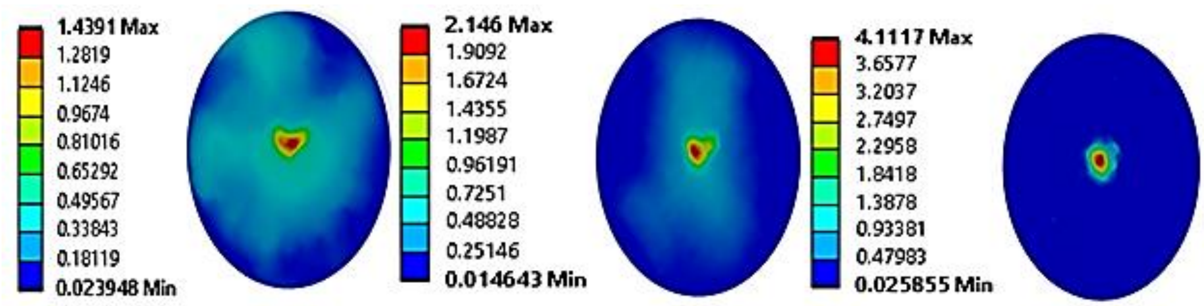

Figure 4-18: Equivalent stress for (a) horizontal (b) 45 degree and (c) vertical orientation

The graphical representation on equivalent stress is shown in Figure 4-19.

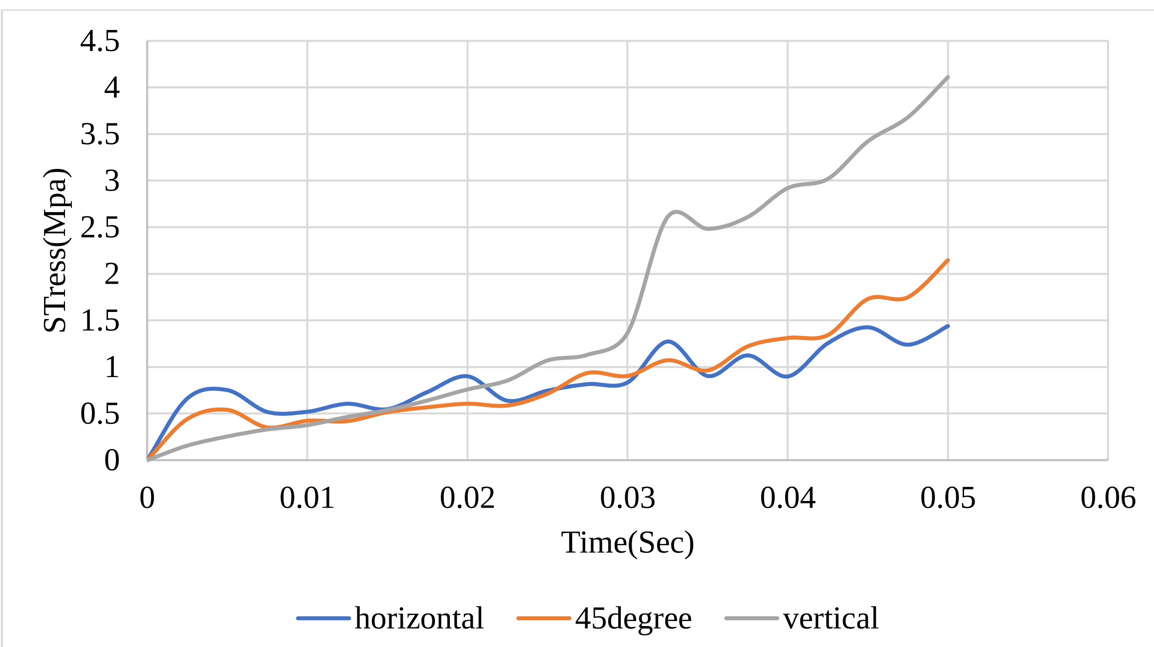

Figure 4-19: Graphical representation of equivalent stress

4.10.2 Total Deformation Result

As shown in figure 4-20 (a) the total deformation is higher on the tip which is the red color which is maximum total deformation is 6.2025mm and minimizing to the center showed by the blue color is the minimum deformation of 1.3887mm. The deformation pattern is concentrated in the center, indicating a significant response to the horizontal. Also, for Figure 4-20 (b) The maximum total deformation is 6.3415mm which is slightly higher than the horizontal case and the minimum is 1.8694mm. For Figure 4-20 (c) The maximum total deformation is 7.3844mm which is the highest among the three cases and the minimum deformation was 4.1556mm. the horizontal print orientation appears to be the favorable print orientation, as it exhibits the lowest maximum total deformation among the three orientations analyzed. Figure 4-21 shows a graphical representation of total deformation.

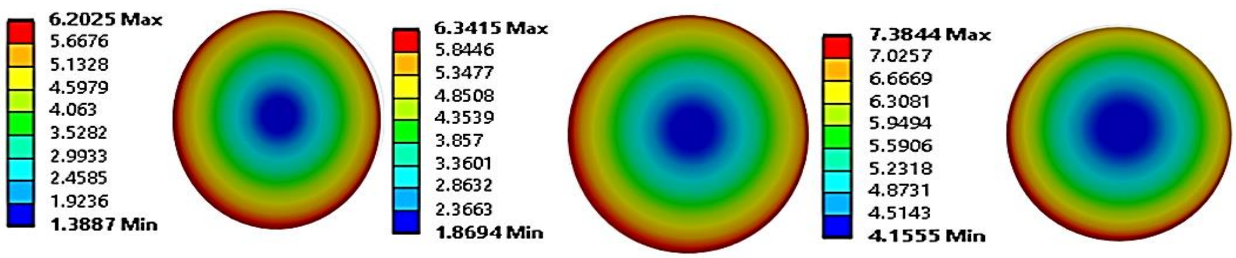

Figure 4-20: total deformation (a) horizontal, (b) 45 degree and (c) vertical orientation

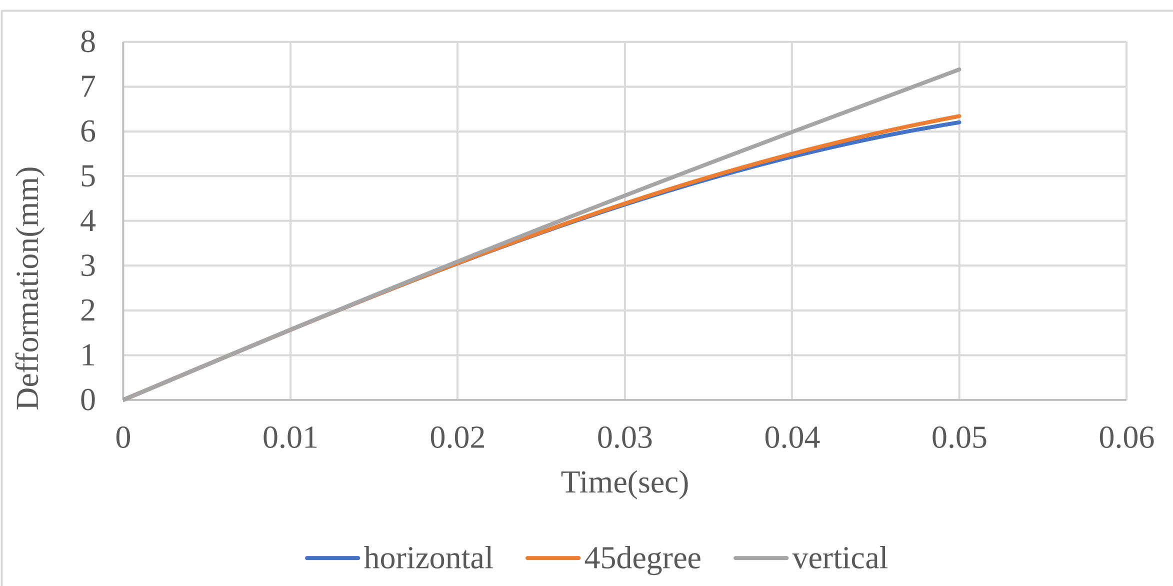

Figure 4-21: Graphical representation of total deformation

CHAPTER FIVE

CONCLUSION AND RECCOMENDATION

5.1 Conclusion

The research aimed to investigate the effects of printing orientation on the mechanical properties and tribological performance of 3D orientation carbon fiber-reinforced polyamide 6 (CFRPA6) were comprehensively investigated. The mechanical properties, specifically hardness and tensile strength, were evaluated for sample orientation in horizontal, vertical, and 45-degree orientations. The tribological properties, including wear rate and coefficient of friction (COF), were analyzed under various conditions. The important findings are drawn based on the results found from the experimental and parametric studies.

1. The experimental results indicate that print orientation significantly affects both the mechanical and tribological properties.
2. Increasing load, sliding speed and track diameter leads to a higher wear rate, specific wear rate and coefficient of friction (COF) in most tests.
3. From the ANOVA, it is observed that the sliding speed significantly influences the multi-performance wear characteristics, with 67.42% for horizontal, 69.88% for vertical, and 56.68% for 45-degree print orientations. This is followed by the applied load, which has an influence of 26.78% for horizontal, 20% for vertical, and 35.78% for 45-degree print orientation. Lastly, the track diameter influences the wear characteristics by 3.05% for horizontal, 8.68% for vertical and 7.27% for 45-degree orientations.
4. The horizontal orientation shows a relatively lower wear rate, specific wear rate, and COF compared to the 45-degree and vertical orientation, especially noticeable in tests for the horizontal print orientation, the minimum effect on wear and COF was observed; for the vertical print orientation, the maximum effect on wear and COF was observed.
5. The optimum result of wear characterization for horizontal, vertical and 45 degrees were wear rate (2.32, 3.23 and 2.45) * 10^{-3} mm^3/m, specific wear rate (2.32, 3.23, and 2.45) * 10^{-4} mm^3/Nm and COF (0.26, 0.35 and 0.29) respectively.
6. The porosity test showed that horizontal orientation relatively lower porosity percentage of 1.03% and vertical 1.73% and 45-degree orientation 1.38%.

7. The horizontal orientation exhibits the highest hardness value at approximately 82 HV, indicating strong resistance to deformation and wear. This is followed by the 45-degree orientation at around 75 HV and the vertical orientation at about 60 HV.
8. The vertical orientation demonstrates the highest tensile strength, with a maximum stress of 0.046019 MPa, indicating better load-bearing capacity and material performance under tension compared to other orientations. the horizontal and 45-degree orientations exhibit lower tensile strengths of 0.019377 MPa and 0.020305 MPa
9. Based on the equivalent stress result the horizontal print orientation has the lowest stress of 1.491MPa, followed by the 45-degree print orientation at 2.146MPa, and the vertical print orientation has the highest stress of 4.117MPa.
10. Based on the maximum total deformation values, the horizontal print orientation has the lowest deformation of 6.2025mm, followed by the 45-degree print orientation at 6.3415mm, and the vertical print orientation has the highest deformation of 7.3844mm.

5.2 Recommendation

Based on the results and conclusions found from this study, the following recommendations were made:

- The horizontal print orientation, recommended for applications that prioritize tribological performance, such as sliding or wear-critical components, exhibits better tribological performance.
- The vertical print orientation demonstrates better overall mechanical performance. For applications focused on superior mechanical properties, such as structural or load-bearing components, the vertical print orientation should be considered.
- The 45-degree print orientation shows intermediate values. Applications with a balance of mechanical and tribological requirements can be recommended.
- In this study, the impact of print orientation was analyzed, and it is suggested to further investigate the influence of other process parameters like layer thickness, infill density, and printing speed on the performance of 3D-oriented CFRPA components.

5.3 Scope for Future Work

- Explore the combined effects of print orientation with other variables such as print speed, layer height, and post-processing treatments.
- Extend the study to evaluate wear performance under varying environmental conditions, such as different temperatures, humidity levels, or exposure to chemicals. This can provide insights into the material's wear resistance in real-world operating environments.
- This research focused on carbon fiber as the reinforcement phase. Other reinforcement forms, such as chopped carbon or hybrid reinforcement (carbon fiber and glass fiber), could lead to further improvements.

Research Fund Acknowledgement

This research project is funded by Adama science and Technology University under the grant number ASTU/SM-R/1044/24, Adama, Ethiopia.

REFERENCE

Abderrafai, Y., Hadi Mahdavi, M., Sosa-Rey, F., Hérard, C., Otero Navas, I., Piccirelli, N., Lévesque, M., & Therriault, D. (2022). Additive manufacturing of short carbon fiber-reinforced polyamide composites by fused filament fabrication: Formulation, manufacturing and characterization. *Materials and Design*, *214*, 110358. https://doi.org/10.1016/j.matdes.2021.110358

Aghababaei, R., Warner, D. H., & Molinari, J. F. (2016). Critical length scale controls adhesive wear mechanisms. *Nature Communications*, *7*. https://doi.org/10.1038/ncomms11816

Ahmad, H., Markina, A. A., Porotnikov, M. V., & Ahmad, F. (2020). A review of carbon fiber materials in automotive industry. *IOP Conference Series: Materials Science and Engineering*, *971*(3). https://doi.org/10.1088/1757-899X/971/3/032011

Ajuka, L. O., Ogedengbe, T. S., Adeyi, T., Ikumapayi, O. M., & Akinlabi, E. T. (2023). Wear characteristics, reduction techniques and its application in automotive parts–A review. In *Cogent Engineering* (Vol. 10, Issue 1). Cogent OA. https://doi.org/10.1080/23311916.2023.2170741

Al Rashid, A., Ikram, H., & Koç, M. (2022). Additive manufacturing and mechanical performance of carbon fiber reinforced Polyamide-6 composites. *Materials Today: Proceedings*, *62*(P12), 6359–6363. https://doi.org/10.1016/j.matpr.2022.03.339

An, H. J., Kim, J. S., Kim, K. Y., Lim, D. Y., & Kim, D. H. (2014). Mechanical and thermal properties of long carbon fiber-reinforced polyamide 6 composites. *Fibers and Polymers*, *15*(11), 2355–2359. https://doi.org/10.1007/s12221-014-2355-5

Bhadauria, N., Pandey, S., & Pandey, P. M. (2019). Wear and enhancement of wear resistance - A review. *Materials Today: Proceedings*, *26*, 2986–2991. https://doi.org/10.1016/j.matpr.2020.02.616

Binder, M., Klocke, F., & Doebbeler, B. (2017). Abrasive wear behavior under metal cutting conditions. *Wear*, *376–377*, 165–171. https://doi.org/10.1016/j.wear.2017.01.065

Botelho, E. C., Figiel, Rezende, M. C., & Lauke, B. (2003a). Mechanical behavior of carbon fiber reinforced polyamide composites. *Composites Science and Technology*, *63*(13), 1843–1855. https://doi.org/10.1016/S0266-3538(03)00119-2

Cai, Z., & Wang, W. (2012). The research on the friction and wear properties of Carbon fiber reinforced polyamide 6 composites. *Applied Mechanics and Materials*, *148–149*, 565–568. https://doi.org/10.4028/www.scientific.net/AMM.148-149.565

Chavhan, G. R., & Wankhade, L. N. (2021). Multiresponse optimization of wear parameters of steel-embedded glass-epoxy hybrid composites using taguchi-grey method optimization. *Materials Performance and Characterization*, *10*(1), 515–531.

Chhabra, D., Deswal, S., Kaushik, A., Garg, R. K., Kovács, A., Khargotra, R., & Singh, T. (2023a). Analysis of fused filament fabrication parameters for sliding wear performance of carbon reinforced polyamide composite material fabricated parts using a hybrid heuristic tool. *Polymer Testing*, *118*(December 2022). https://doi.org/10.1016/j.polymertesting.2022.107910

Chockalingam, S., Subramaniyan, G. G., Bisen, A., Kaliappan, S., Sekar, S., Patil, P. P., Kumar, T. C. A., Ramesh, B., & Venkatesan, S. (2022). Optimization of Abrasive Wear Characteristics of Polyethylene/Acrylate Copolymer Nanocomposites. *Advances in Materials Science and Engineering*, *2022*. https://doi.org/10.1155/2022/6110591

ÇOBAN, S., & OKTAY, T. (2023). Innovative Morphing UAV Design and Manufacture. *Journal of Aviation*, *7*(2), 184–189. https://doi.org/10.30518/jav.1253901

Dangnan, F., Espejo, C., Liskiewicz, T., Gester, M., & Neville, A. (2020). Friction and wear of additive manufactured polymers in dry contact. *Journal of Manufacturing Processes*, *59*, 238–247. https://doi.org/10.1016/j.jmapro.2020.09.051

Dhakal, N., Espejo, C., Morina, A., & Emami, N. (2024). Tribological performance of 3D printed neat and carbon fiber reinforced PEEK composites. *Tribology International*, *193*. https://doi.org/10.1016/j.triboint.2024.109356

Dong, F., Hou, G., Liu, H., Liu, L., Cao, F., Wang, J., & Yan, F. (2018). An investigation on the mechanical and tribological properties of carbon fiber/polyimide composites at elevated temperatures. *Polymer Composites*, *39*, E869–E882. https://doi.org/10.1002/pc.24290

Dul, S., Fambri, L., & Pegoretti, A. (2021). High-Performance Polyamide/Carbon Fiber Composites for Fused Filament Fabrication: Mechanical and Functional Performances. *Journal of Materials Engineering and Performance*, *30*(7), 5066–5085. https://doi.org/10.1007/s11665-021-05635-1

Espadinha-Cruz, P., Neves, A., Matos, F., & Godina, R. (2023). Development of a maturity model for additive manufacturing: A conceptual model proposal. *Heliyon*, *9*(5). https://doi.org/10.1016/j.heliyon.2023.e16099

Gadelmoula, A., & Aldahash, S. A. (2023). Effect of Reinforcement with Short Carbon Fibers on the Friction and Wear Resistance of Additively Manufactured PA12. *Polymers*, *15*(15). https://doi.org/10.3390/polym15153187

Gajalakshmi, K., Senthilkumar, N., & Prabu, B. (2019). Multi-response optimization of dry sliding wear parameters of AA6026 using hybrid gray relational analysis coupled with response surface method. *Measurement and Control (United Kingdom)*, *52*(5–6), 540–553. https://doi.org/10.1177/0020294019842603

Gangaraju, Srivastava, A., & Ramesh, C. S. (2023). Joining of Nylon Using Friction Stir Welding (FSW) Techniques. *SAE Technical Papers, January*, 0–11. https://doi.org/10.4271/2023-01-0994

Gan, X., Fei, G., Wang, J., Wang, Z., Lavorgna, M., & Xia, H. (2020). Powder quality and electrical conductivity of selective laser sintered polymer composite components. In *Structure and Properties of Additive Manufactured Polymer Components* (pp. 149–185). Elsevier.

Gao, J., Li, B., Bu, H., Li, X., & Zhan, X. (2023). Effect of infill density and reinforced perimeters on tensile properties and fracture mechanism of 3D printing carbon fiber–reinforced composite. *International Journal of Advanced Manufacturing Technology*, *128*(1–2), 267–281. https://doi.org/10.1007/s00170-023-11871-7

Gueche, Y. A., Sanchez-Ballester, N. M., Cailleaux, S., Bataille, B., & Soulairol, I. (2021). Selective laser sintering (Sls), a new chapter in the production of solid oral forms (sofs) by 3d printing. In *Pharmaceutics* (Vol. 13, Issue 8). MDPI AG. https://doi.org/10.3390/pharmaceutics13081212

Hanief, M., & Charoo, M. S. (2021). Archard's wear law revisited to measure accurate wear coefficient considering actual sliding velocity. *Materials Today: Proceedings*, *47*, 5598–5600.

Hanon, M. M., Marczis, R., & Zsidai, L. (2020). Impact of 3D-printing structure on the tribological properties of polymers. *Industrial Lubrication and Tribology*, *72*(6), 811–818. https://doi.org/10.1108/ILT-05-2019-0189

Hao, W., Liu, Y., Zhou, H., Chen, H., & Fang, D. (2018). Preparation and characterization of 3D printed continuous carbon fiber reinforced thermosetting composites. *Polymer Testing*, *65*(September 2017), 29–34. https://doi.org/10.1016/j.polymertesting.2017.11.004

Hendlmeier, A., Simon, Ž., Wickramasingha, Y. A., & Henderson, L. C. (2021). A comparison of compression molded and additively manufactured short carbon fiber reinforced polyamide-6 samples and the effect of different infill printing patterns. *Polymer Composites*, *42*(9), 4728–4735. https://doi.org/10.1002/pc.26182

Jin, Y. A., Li, H., He, Y., & Fu, J. Z. (2015). Quantitative analysis of surface profile in fused deposition modelling. *Additive Manufacturing*, *8*, 142–148. https://doi.org/10.1016/j.addma.2015.10.001

Kausar, A. (2019). Advances in Carbon Fiber Reinforced Polyamide-Based Composite Materials. *Advances in Materials Science*, *19*(4), 67–82. https://doi.org/10.2478/adms-2019-0023

Krishna Vamsi, A. A., S Deva Kumar, M. L., V Sai Ram, Y. N., Graduate, P., & Andhra Pradesh, G. (2022). APPLICATION OF TAGUCHI BASED GREYRELATION ANALYSIS TO STUDY DRY-SLIDING WEAR PARAMETERS ON CARBON FIBER REINFORCED EPOXY COMPOSITES. In *Peer Reviewed and Refereed Journal* (Issue 3). http://ijmer.in/pdf/e-Certificate%20of%20Publication-IJMER.pdf

Kumar, A., Choudhary, A., Tiwari, A., James, C., Kumar, H., Kumar Arora, P., & Akhtar Khan, S. (2021a). An investigation on wear characteristics of additive manufacturing materials. *Materials Today: Proceedings*, *47*(xxxx), 3654–3660. https://doi.org/10.1016/j.matpr.2021.01.263

Le Gentil, T., Langot, J., Therriault, D., & Kerbrat, O. (2023). Identifying efficient solutions for additive manufacturing of short carbon-fiber reinforced polyamide 6 from energy and mechanical perspectives. *Procedia CIRP*, *116*, 540–545. https://doi.org/10.1016/j.procir.2023.02.091

Li, J., & Xia, Y. C. (2009). The reinforcement effect of carbon fiber on the friction and wear properties of carbon fiber reinforced PA6 composites. *Fibers and Polymers*, *10*(4), 519–525. https://doi.org/10.1007/s12221-009-0519-5

Lupone, F., Padovano, E., Venezia, C., & Badini, C. (2022). Experimental Characterization and Modeling of 3D Printed Continuous Carbon Fibers Composites with Different Fiber

Orientation Produced by FFF Process. *Polymers*, *14*(3). https://doi.org/10.3390/polym14030426

Mudhaffer, S., Althagafi, R., Haider, J., Satterthwaite, J., & Silikas, N. (2024). Effects of printing orientation and artificial ageing on martens hardness and indentation modulus of 3D printed restorative resin materials. *Dental Materials*.

Muthu, P. (2020). Multi objective optimization of wear behaviour of Aluminum MMCs using Grey-Taguchi method. *Manufacturing Review*, *7*. https://doi.org/10.1051/mfreview/2020013

Naik, M., Thakur, D. G., Chandel, S., Salunkhe, S., & Hussein, H. M. A. (2022c). Effect of Load and Fiber Orientation on Wear Properties of Additively Manufactured Continuous CFRP Composites under Dry Sliding Conditions. *Crystals*, *12*(10). https://doi.org/10.3390/cryst12101481

Naima Khalid, N., Afiqah Mohd Radzuan, N., Bakar Sulong, A., & Mohd Foudzi, F. (2021). A review on bonding of Polyamide reinforced carbon fibre via additive manufacturing. *IOP Conference Series: Materials Science and Engineering*, *1078*(1), 012004. https://doi.org/10.1088/1757-899x/1078/1/012004

Negi, S., Kumar Sharma, R., & Dhiman, S. (2013). Basics, applications and future of additive manufacturing technologies: A review. *Article in Journal of Manufacturing Technology Research · March*, *5*(1). https://www.researchgate.net/publication/281004567

Norani, M. N. M., Abdullah, M. I. H. C., Abdollah, M. F. Bin, Amiruddin, H., Ramli, F. R., & Tamaldin, N. (2021a). Mechanical and tribological properties of fff 3d-printed polymers: A brief review. *Jurnal Tribologi*, *29*(April), 11–30.

Odabas, D. (2018). Effects of Load and Speed on Wear Rate of Abrasive Wear for 2014 Al Alloy. *IOP Conference Series: Materials Science and Engineering*, *295*(1). https://doi.org/10.1088/1757-899X/295/1/012008

Papa, I., Silvestri, A. T., Ricciardi, M. R., Lopresto, V., & Squillace, A. (2021). *Effect of Fibre Orientation on Novel Continuous 3D-Printed Fibre-Reinforced Composites*. https://doi.org/10.3390/polym

Pejkowski, Ł., Seyda, J., Nowicki, K., & Mrozik, D. (2023). Mechanical performance of non-reinforced, carbon fiber reinforced and glass bubbles reinforced 3D printed PA12 polyamide. *Polymer Testing*, *118*(December 2022), 1–11. https://doi.org/10.1016/j.polymertesting.2022.107891

Peng, Y., Wu, Y., Li, S., Wang, K., Yao, S., Liu, Z., & Garmestani, H. (2020). Tailorable rigidity and energy-absorption capability of 3D printed continuous carbon fiber reinforced polyamide composites. *Composites Science and Technology*, *199*(February), 108337. https://doi.org/10.1016/j.compscitech.2020.108337

Pereira, A. A. C., & d'Almeida, J. R. M. (2023). Wear behavior of polyamide 11 reinforced with titanate nanotubes. *Journal of Thermoplastic Composite Materials*, *36*(2), 510–534. https://doi.org/10.1177/08927057211013391

Popov, V. L., & Psakhie, S. G. (2007). Numerical simulation methods in tribology. *Tribology International*, *40*(6), 916–923. https://doi.org/10.1016/j.triboint.2006.02.020

Prabhu, P., Suresh Kumar, M., Singh, P., Siva, & K., & Singh, A. P. (2014). Experimental Study and Verification of Wear for Glass Reinforced Polymer using ANSYS. *Type: Double Blind Peer Reviewed International Research Journal Publisher: Global Journals Inc*, *14*.

Prajapati, P. K., Kumar, S., & Singh, K. K. (2020). Optimization of Tribological Behavior of CFRP Composites under dry sliding condition using Taguchi Method. In *Materials Today: Proceedings* (Vol. 21). www.sciencedirect.comwww.materialstoday.com/proceedings2214-7853

Ranganathan, S., Kumar K, S., Gopal, S., & Pradeep, C. (2020). The Effect of Print Orientation and Infill Density for 3D Printing on Mechanical and Tribological Properties. *SAE Technical Papers*, *2020*. https://doi.org/10.4271/2020-28-0411

Rankouhi, B., Javadpour, S., Delfanian, F., & Letcher, T. (2016). Failure Analysis and Mechanical Characterization of 3D Printed ABS With Respect to Layer Thickness and Orientation. *Journal of Failure Analysis and Prevention*, *16*(3), 467–481. https://doi.org/10.1007/s11668-016-0113-2

Sanei, S. H. R., & Popescu, D. (2020). 3d-printed carbon fiber reinforced polymer composites: A systematic review. *Journal of Composites Science*, *4*(3). https://doi.org/10.3390/jcs4030098

Shen, X., Cao, L., & Li, R. (2010). Numerical simulation of sliding wear based on archard model. *2010 International Conference on Mechanic Automation and Control Engineering*, 325–329.

Singh, S., Sachdeva, A., & Sharma, V. S. (2012). A STUDY ON SELECTIVE LASER SINTERED PARTS FOR DIMENSIONAL AND SURFACE CHARACTERISTICS. *Journal of Manufacturing Technology Research*, *4*.

Solomon, I. J., Sevvel, P., & Gunasekaran, J. (2020). A review on the various processing parameters in FDM. *Materials Today: Proceedings*, *37*(Part 2), 509–514. https://doi.org/10.1016/j.matpr.2020.05.484

Sylajakumari, P. A., Ramakrishnasamy, R., & Palaniappan, G. (2018). Taguchi grey relational analysis for multi-response optimization of wear in co-continuous composite. *Materials*, *11*(9). https://doi.org/10.3390/ma11091743

Tian, X., Liu, T., Yang, C., Wang, Q., & Li, D. (2016). Interface and performance of 3D printed continuous carbon fiber reinforced PLA composites. *Composites Part A: Applied Science and Manufacturing*, *88*, 198–205. https://doi.org/10.1016/j.compositesa.2016.05.032

Todoroki, A., Oasada, T., Mizutani, Y., Suzuki, Y., Ueda, M., Matsuzaki, R., & Hirano, Y. (2020). Tensile property evaluations of 3D printed continuous carbon fiber reinforced thermoplastic composites. *Advanced Composite Materials*, *29*(2), 147–162. https://doi.org/10.1080/09243046.2019.1650323

Tymrak, B. M. M., Kreiger, M., & Pearce, J. M. (2014). Mechanical properties of components fabricated with open-source 3-D printers under realistic environmental conditions. *Materials & Design*, *58*. https://doi.org/10.1016/j.matdes.2014.02.038ï

Unal, H., & Mimaroglu, A. (2012a). Friction and wear performance of polyamide 6 and graphite and wax polyamide 6 composites under dry sliding conditions. *Wear*, *289*, 132–137. https://doi.org/10.1016/j.wear.2012.04.004

Unal, H., & Mimaroglu, A. (2012b). Friction and wear performance of polyamide 6 and graphite and wax polyamide 6 composites under dry sliding conditions. *Wear*, *289*, 132–137. https://doi.org/10.1016/j.wear.2012.04.004

Venoor, V., Park, J. H., Kazmer, D. O., & Sobkowicz, M. J. (2021). Understanding the Effect of Water in Polyamides: A Review. In *Polymer Reviews* (Vol. 61, Issue 3, pp. 598–645). Taylor and Francis Ltd. https://doi.org/10.1080/15583724.2020.1855196

Zhang, X., Yang, H., Zhang, H., & Wang, C. (2012). A carbon fiber reinforced nylon 6 (CFRPA6) composite specialized for military field cooking task. *Applied Mechanics and Materials*, *224*, 199–203. https://doi.org/10.4028/www.scientific.net/AMM.224.199

Zhou, S., Zhang, Q., Wu, C., & Huang, J. (2013). Effect of carbon fiber reinforcement on the mechanical and tribological properties of polyamide6/polyphenylene sulfide composites. *Materials and Design*, *44*, 493–499. https://doi.org/10.1016/j.matdes.2012.08.029

APPENDIX- I: Figures

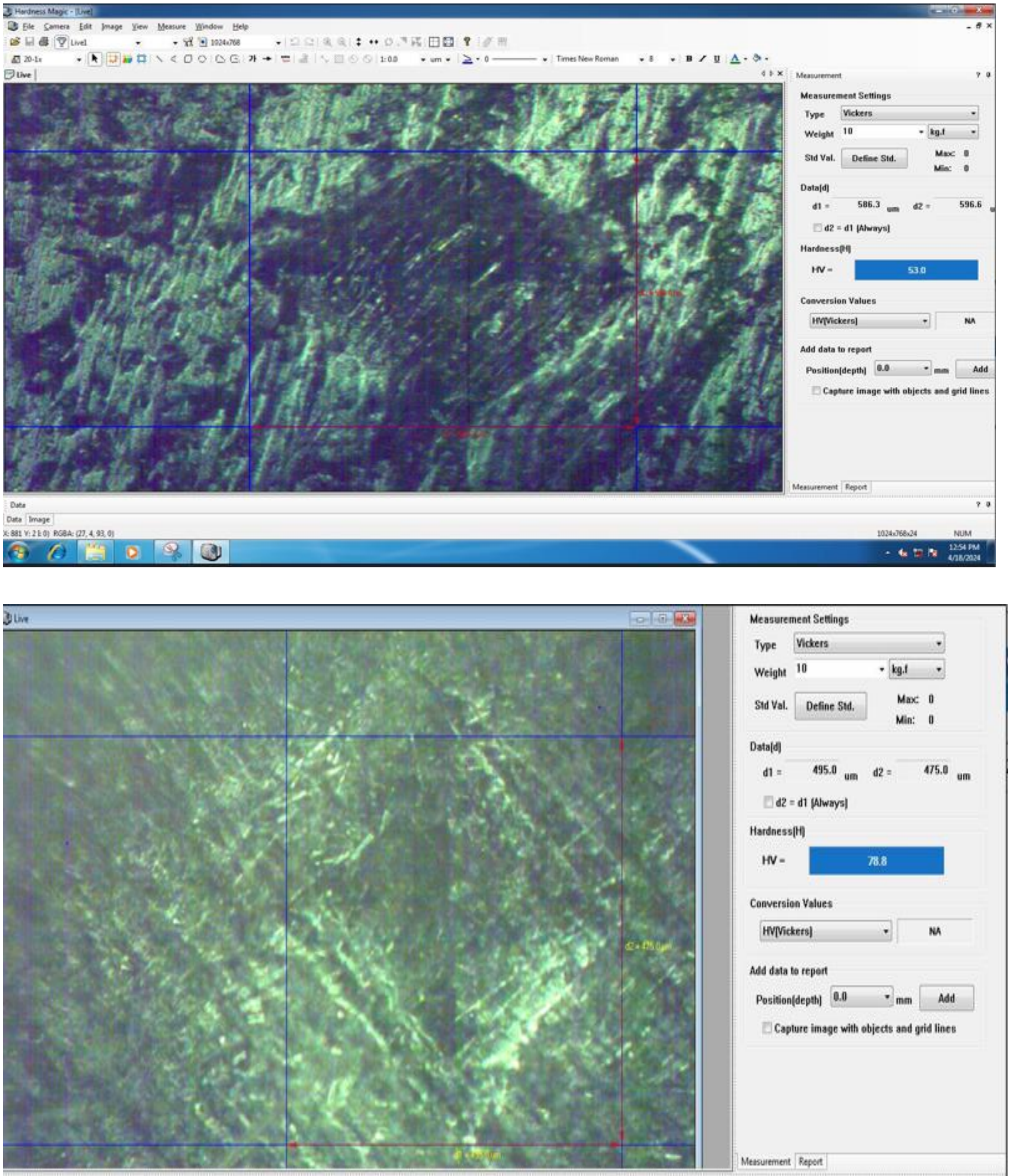

Figure A-1 Micro hardness Vickers value

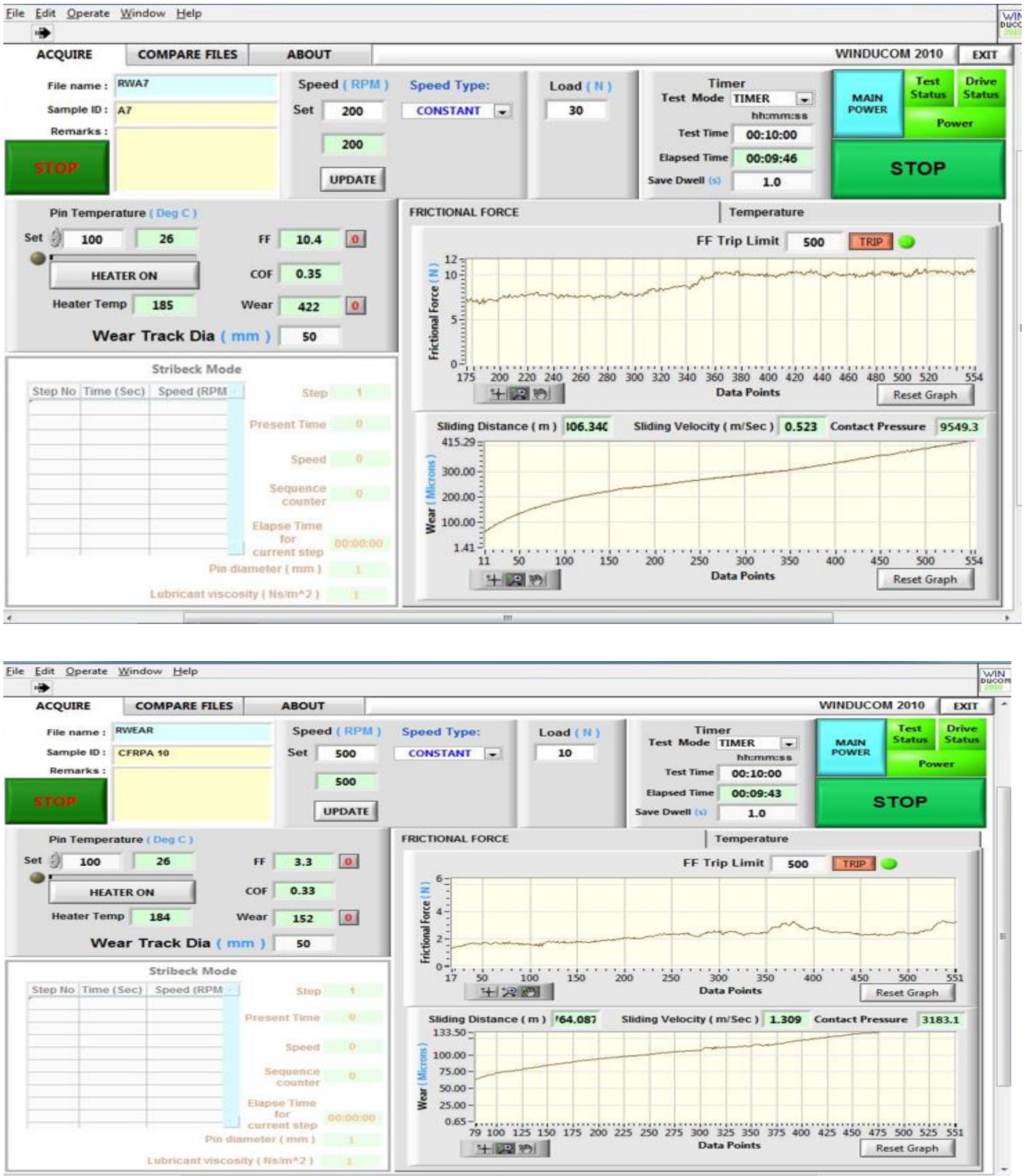

Figure A-2: Graph of the wear test setup

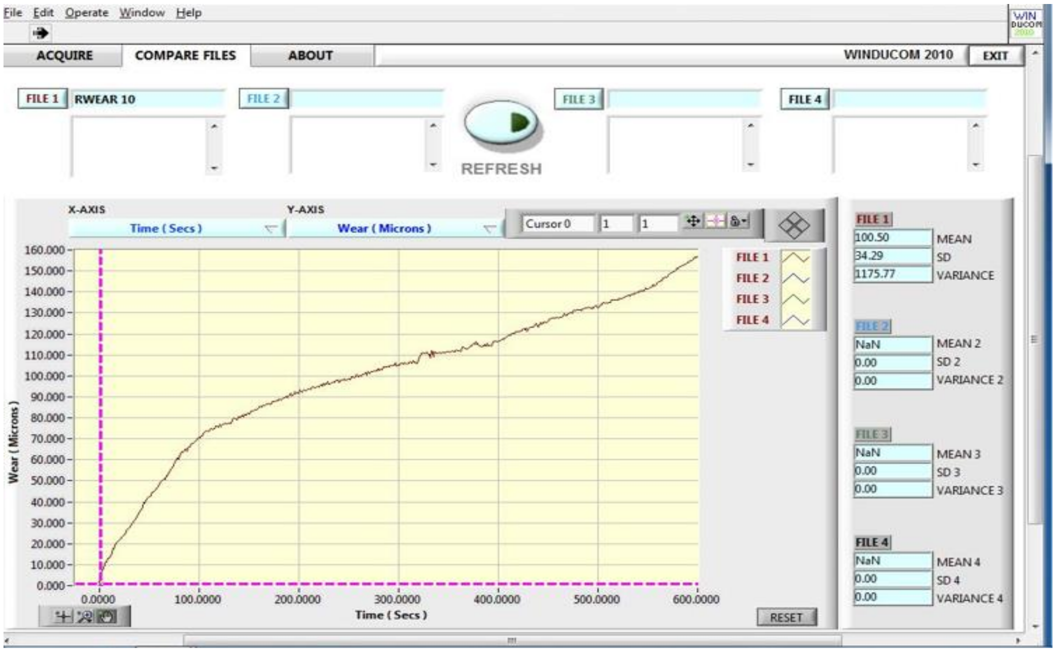

Figure A-3: Graph of wear Vs time

Figure A-4: Graph of coefficient of friction Vs time

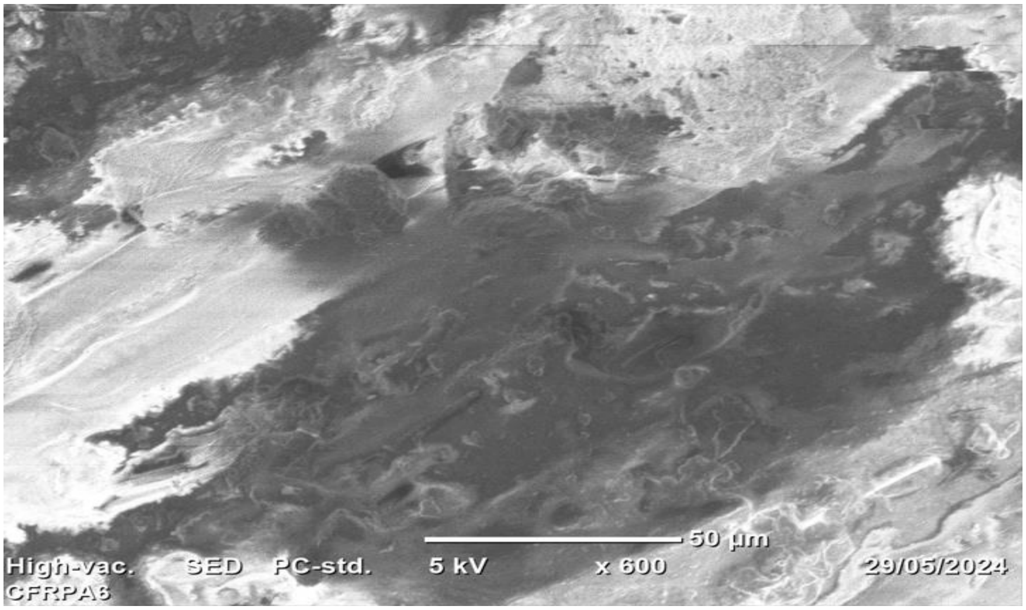

Figure A-5: SEM image of worn surface

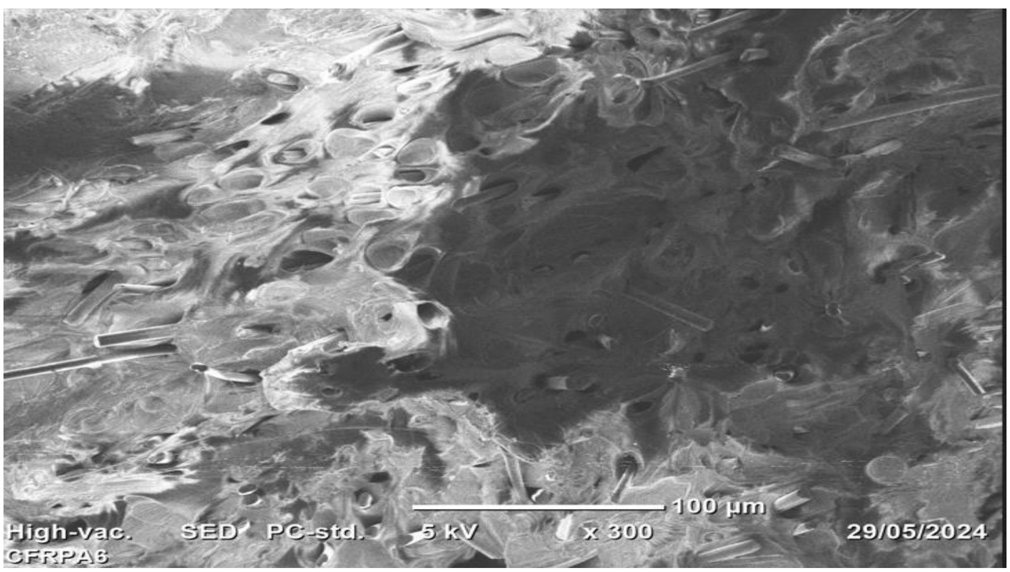

Figure A-6: SEM analysis of fracture surface after tensile test

APPENDIX II: Table of deformation and stress

Table A-1: Deformation and stress result from LS-DYNA simulation

T(sec)	Deformation (mm)			Stress (MPa)		
	horizontal	45degree	vertical	horizontal	45degree	vertical
0	0	0	0	0	0	0
2.50E-03	0.39285	0.3929	0.39312	0.66045	0.43985	0.15544
5.00E-03	0.78615	0.78638	0.78716	0.7519	0.53982	0.25377
7.50E-03	1.1771	1.1776	1.1788	0.51754	0.35137	0.32932
1.00E-02	1.5651	1.5658	1.5676	0.5192	0.42272	0.37543
1.25E-02	1.9479	1.949	1.9532	0.60515	0.41897	0.46385
1.50E-02	2.3236	2.3253	2.3355	0.54658	0.51555	0.53701
1.75E-02	2.6918	2.6948	2.7154	0.73099	0.5674	0.64041
2.00E-02	3.0507	3.0556	3.0926	0.90022	0.60551	0.75865
2.25E-02	3.3985	3.4063	3.4661	0.63746	0.58634	0.8549
2.50E-02	3.7347	3.7462	3.8364	0.74605	0.71331	1.0696
2.75E-02	4.0576	4.0741	4.2027	0.81576	0.93541	1.131
3.00E-02	4.3658	4.3881	4.5651	0.83355	0.90367	1.366
3.25E-02	4.5587	4.5889	4.9248	1.2728	1.0722	2.6093
3.50E-02	4.9352	4.9744	5.2814	0.90322	0.96347	2.4828
3.75E-02	5.1937	5.2439	5.6342	1.1242	1.221	2.6093
4.00E-02	5.4343	5.4975	5.9852	0.89852	1.3113	2.9195
4.25E-02	5.6561	5.7341	6.3347	1.2547	1.3418	3.0189
4.50E-02	5.8582	5.9538	6.6835	1.4257	1.7294	3.4208
4.65E-02	6.0404	6.1561	7.033	1.2391	1.7481	3.6796
5.00E-02	6.2023	6.3413	7.384	1.4391	2.146	4.1117
5.00E-02	6.2025	6.3415	7.3844	1.4391	2.146	4.1117